J. Fluid Mech. (1988), *vol.* 188, *pp.* 47–85
Printed in Great Britain

The breakdown of steady convection

By T. B. LENNIE
BP Exploration Co. Ltd, Britannic House, London EC2Y 9BU, UK

D. P. McKENZIE
Department of Earth Sciences, University of Cambridge, Cambridge CB3 0EZ, UK

D. R. MOORE
Department of Mathematics, Imperial College, London SW7 2BZ, UK

AND N. O. WEISS
Department of Applied Mathematics and Theoretical Physics, University of Cambridge, Cambridge CB3 9EW, UK

(Received 12 May 1986 and in revised form 27 May 1987)

Two-dimensional convection in a Boussinesq fluid with infinite Prandtl number, confined between rigid horizontal boundaries and stress-free lateral boundaries, has been investigated in a series of numerical experiments. In a layer heated from below steady convection becomes unstable to oscillatory modes caused by the formation of hot or cold blobs in thermal boundary layers. Convection driven by internal heating shows a transition from steady motion through periodic oscillations to a chaotic regime, owing to the formation of cold blobs which plunge downwards and eventually split the roll. The interesting feature of this idealized problem is the interaction between constraints imposed by nonlinear dynamics and the obvious spatial structures associated with the sinking sheets and changes in the preferred cell size. These spatial structures modify the bifurcation patterns that are familiar from transitions to chaos in low-order systems. On the other hand, even large-amplitude disturbances are constrained to show periodic or quasi-periodic behaviour, and the bifurcation sequences can be followed in considerable detail. There are examples of quasi-periodic behaviour followed by intermittency, of period-doubling cascades and of transitions from quasi-periodicity to chaos, associated with a preference for narrower rolls as the Rayleigh number is increased.

1. Introduction

Recent advances in the theory of dynamical systems have transformed our understanding of nonlinear dissipative processes. Although their bearing on turbulence has been much exaggerated, these results do have important fluid dynamical applications. In particular, they illuminate various aspects of nonlinear convection (Normande, Pomeau & Velarde 1977; Busse 1978, 1981; Bergé, Pomeau & Vidal 1984; Guckenheimer 1986). So far, most studies have focused on complicated temporal behaviour in systems with essentially simple spatial patterns (e.g. Arnéodo, Coullet & Spiegel 1985; Knobloch *et al.* 1986). In this paper we shall explore more complicated spatial structures and see how bifurcations and transitions to chaos are related to changes in the pattern of cellular convection.

In the nonlinear regime, bifurcations may lead to loss of symmetry or changes in

planform. These may be soft transitions (corresponding to supercritical bifurcations) as exemplified by symmetry breaking in two-dimensional magnetoconvection (Weiss 1981) or three-dimensional Bénard convection (T. B. Lennie, D. P. McKenzie, D. R. Moore & N. O. Weiss, in preparation). Alternatively, there may be discontinuous changes of cell form in systems that are laterally constrained. Such transitions are associated with hysteresis and subcritical bifurcations. Two techniques are available for studying this behaviour in idealized configurations: the relevant partial differential equations can be integrated numerically, or the appropriate normal form equations can be derived and analysed (e.g. Knobloch & Guckenheimer 1983; Fauve 1985). We shall investigate systems in which there is a transition from steady convection to complicated time-dependent behaviour, associated with changes in cell size, by means of numerical experiments. Although such computational studies are limited to idealized theoretical configurations which cannot be realized experimentally they do illuminate the interaction between spatial structure and the constraints imposed by nonlinear dynamics.

Our aim is to isolate a particular effect and then to understand it. In our models, time dependence is associated with the formation of hot or cold blobs in unstable thermal boundary layers. We seek to relate this obvious physical behaviour to mathematical results from dynamical systems theory. A similar instability arises for convection in a closed tube that is heated differentially (Keller 1966; Welander 1967); indeed, motion in a circular tube is actually described by the Lorenz equations (Malkus 1972). Moreover, Krishnamurti (1970), Bergé & Dubois (1979) and Walden *et al.* (1984) have detected oscillations in laboratory experiments on convection which they ascribe to hot and cold blobs circulating round the cells. Similar oscillations have been found in numerical investigations of two-dimensional convection in a layer heated from below (Moore & Weiss 1973*a*; Curry *et al.* 1984). The Lorenz (1963) equations were originally derived from the lowest-order non-trivial approximation for this problem: after the initial bifurcation from a static solution to a branch of steadily convecting solutions, there is a subcritical oscillatory bifurcation, followed by chaos (Sparrow 1982). As more terms are included in the Galerkin approximation, generating higher-order systems of equations, solutions no longer display the rich time-dependent behaviour characteristic of the Lorenz system (Veronis 1966; Curry 1978; Maschke & Saramito 1982; Treve & Manley 1982; Curry *et al.* 1984). Accurate numerical solutions of the partial differential equations retain a supercritical oscillatory bifurcation, followed by periodic or doubly periodic motion but with no hint of chaos (Moore & Weiss 1973*a*; Curry *et al.* 1984). Reliable numerical studies of two-dimensional convection in a porous medium do, however, show periodic, quasi-periodic and chaotic oscillations (Kimura, Schubert & Straus 1986).

Chaotic behaviour also appears in numerical experiments on convection driven by internal heating (McKenzie, Roberts & Weiss 1974). We shall study two-dimensional Boussinesq convection in a layer confined by rigid horizontal surfaces and stress-free lateral boundaries, for a fluid with infinite Prandtl number (motivated by geophysical considerations). When the layer is heated from within, a thermal boundary layer forms at the top and motion is dominated by cold sinking plumes. As the rate of heating is increased there is first a stationary bifurcation (corresponding to the onset of steady cellular convection) and then an oscillatory bifurcation (when the boundary layer becomes unstable). Cold blobs form, producing oscillations as they circulate around the cell. These oscillations become aperiodic and grow more violent

until the cell eventually splits. The artificial restriction to two-dimensional flow allows us to follow the transition from periodicity to chaos, through quasi-periodic motion and cascades of period-doubling bifurcations, in considerable detail. At each stage the dynamics characteristic of low-order systems can be related to the physical behaviour of the temperature and velocity in a cell. Moreover, this simple problem has the property that the horizontal scale of motion diminishes as the rate of heating is increased, making it an interesting model for other, more complicated fluid systems.

In the next section we present the relevant equations and describe the techniques used to solve them. Then, in §3, we discuss convection in a layer heated from below and show how unstable thermal boundary layers lead to oscillations about a steadily convecting state. Thereafter, we concentrate on convection in a layer heated entirely from within, with a fixed temperature at the upper boundary. In §4 we treat convection in a roll with square cross-section, where there is a bifurcation from periodic to quasi-periodic behaviour, followed by a homoclinic bifurcation and an abrupt transition into chaos. This is the first time that such a transition (involving a strong resonance, period-doubling and intermittency) has been analysed in any detail. In §5 we study convection in a wider cell, where the ratio of roll width to layer depth $\lambda = 1.5$; there chaos appears after a period-doubling cascade and periodic windows are related to resonances in the two-dimensional flow. In §6 we investigate narrow cells, with $\lambda = 0.5$, 0.75, and look at instabilities that appear in a layer containing several rolls. Finally, in §7, we summarize the mathematical and physical features of our results and comment on the behaviour that might be expected as more and more spatial scales are excited.

2. Two-dimensional convection

2.1. *The model problem*

We consider two-dimensional convection in a Boussinesq fluid occupying the region $\{0 < x < \lambda d;\ 0 < z < d\}$, referred to Cartesian coordinates with the z-axis pointing upwards. The velocity $\boldsymbol{u}$ is solenoidal and the vorticity, $\boldsymbol{\omega} = \operatorname{curl} \boldsymbol{u} = (0, \omega, 0)$; hence we introduce a stream function ψ such that

$$\boldsymbol{u} = (u, 0, w) = \left(-\frac{\partial \psi}{\partial z}, 0, \frac{\partial \psi}{\partial x}\right), \quad \omega = -\nabla^2 \psi. \tag{2.1}$$

Then conservation of energy requires that the temperature T satisfies the equation

$$\frac{\partial T}{\partial t} + \boldsymbol{\nabla} \cdot (T\boldsymbol{u}) = \epsilon + \kappa \nabla^2 T, \tag{2.2}$$

where ϵ is the thermometrical internal heating rate, while vorticity evolves according to the equation

$$\frac{\partial \omega}{\partial t} + \boldsymbol{\nabla} \cdot (\omega \boldsymbol{u}) = -g\alpha \frac{\partial T}{\partial x} + \nu \nabla^2 \omega. \tag{2.3}$$

Here κ, ν are the thermal and viscous diffusivities, α is the coefficient of thermal expansion and g is the gravitational acceleration. When the Prandtl number, $\sigma = \nu/\kappa$, is very large (as in the Earth's mantle) the inertial terms on the left-hand side of (2.3) can be ignored. Then, measuring distances and times in terms of the layer depth

d and the thermal diffusion time d^2/κ, respectively, we obtain the dimensionless equations

$$\frac{\partial T}{\partial t} = \frac{\partial(T, \psi)}{\partial(x, z)} + \epsilon_0 + \nabla^2 T, \tag{2.4}$$

$$\nabla^2 \omega = R\frac{\partial T}{\partial x}, \tag{2.5}$$

where the Rayleigh number

$$R = \frac{g\alpha \Delta T d^3}{\kappa \nu}, \tag{2.6}$$

and temperature is measured in terms of a characteristic temperature difference ΔT imposed across the layer, while the dimensionless internal heating rate

$$\epsilon_0 = \frac{\epsilon d^2}{\kappa \Delta T}. \tag{2.7}$$

For infinite Prandtl number the only nonlinearity is produced by advection of temperature in (2.4), and the stream function satisfies the biharmonic equation

$$\nabla^4 \psi = -R\frac{\partial T}{\partial x}, \tag{2.8}$$

from (2.1) and (2.5). We impose rigid, no-slip boundary conditions at the top and bottom of the layer, and assume that the lateral boundaries are free, so that

$$\left.\begin{aligned} \psi = 0 \quad (x = 0, \lambda; \quad z = 0, 1), \\ \frac{\partial \psi}{\partial z} = 0 \quad (z = 0, 1); \quad \frac{\partial^2 \psi}{\partial x^2} = 0 \quad (x = 0, \lambda). \end{aligned}\right\} \tag{2.9}$$

In what follows we assume that the upper boundary is maintained at a fixed temperature (set arbitrarily to zero) and fix either the temperature or the heat flux at the lower boundary. For a fixed temperature T_0 at the lower boundary, $\Delta T = T_0 + \epsilon d^2/2\kappa$. For a fixed heat flux f across the lower boundary, $\Delta T = (d/\kappa)(f + \epsilon d)$. In particular, for a layer heated entirely from below $\epsilon_0 = 0$, while for a layer heated entirely from within $\epsilon_0 = 1$, from (2.7). The dimensionless temperature satisfies the boundary conditions

$$T = 0 \quad (z = 1), \qquad \frac{\partial T}{\partial x} = 0 \quad (x = 0, \lambda) \tag{2.10}$$

and either (for fixed temperature)

$$T = 1 - \tfrac{1}{2}\epsilon_0 \quad (z = 0) \tag{2.11}$$

or (for fixed flux)

$$\frac{\partial T}{\partial z} = -(1 - \epsilon_0) \quad (z = 0). \tag{2.12}$$

Thus we must solve the parabolic differential equation (2.4) together with the elliptic equation (2.8), subject to the boundary conditions (2.9), (2.10) and (2.11) or (2.12).

It is useful to introduce global measures of the vigour of nonlinear convection. One such quantity is the mean kinetic energy

$$E = (2\lambda)^{-1} \int_0^1 \int_0^\lambda |\boldsymbol{u}|^2 \, dx \, dz = (2\lambda)^{-1} \int_0^1 \int_0^\lambda \psi \omega \, dx \, dz, \tag{2.13}$$

	B.c. at $z = 0$	ϵ_0	R_c	λ_c	a_c
(*a*)	$T = 1$	0	1708	1.008	3.12
(*b*)	$\partial T/\partial z = -1$	0	1296	1.23	2.55
(*c*)	$T = \frac{1}{2}$	1	3390	1.005	3.13
(*d*)	$\partial T/\partial z = 0$	1	2772	1.19	2.63

TABLE 1. Critical Rayleigh numbers for marginal stability (fixed boundaries, $T = 0$ at $z = 1$)

which is zero in the absence of motion. Another is the Nusselt number N, which provides a dimensionless measure of the heat flux. Let

$$T_0 = \lambda^{-1} \int_0^\lambda T(x, 0)\, \mathrm{d}x \tag{2.14}$$

be the mean temperature at the lower boundary. Then

$$N = -(\lambda T_0)^{-1} \int_0^\lambda \left. \frac{\partial T}{\partial z} \right|_{(z=1)} \mathrm{d}x \tag{2.15}$$

is the ratio of the actual heat flux to that which would have been carried in the absence of convection, had the temperature gradient been uniform. For a layer heated entirely from below, $(N-1)$ measures the convective flux.

2.2. *Linear stability*

Equations (2.4) and (2.8) possess a static, purely convecting solution with $\psi = \omega = 0$. For a layer heated entirely from below this solution has a uniform temperature gradient so that $T = 1-z$. If the layer is heated entirely from within then the temperature has a parabolic profile with

$$T = \tfrac{1}{2}(1-z^2). \tag{2.16}$$

When this solution is perturbed we suppose that either the temperature or the vertical temperature gradient remains fixed at the lower boundary. In each case the trivial, conducting solution undergoes a supercritical stationary bifurcation at some Rayleigh number $R_0(\lambda)$. As λ is varied, R_0 attains a minimum value for $\lambda = \lambda_c$ and $R_c = R_0(\lambda_c)$. Table 1 shows the values of R_c, λ_c and the horizontal wavenumber $a_c = \pi/\lambda_c$, for the four cases that we shall consider (Chandrasekhar 1961; Sparrow, Goldstein & Jonsson 1964; Roberts 1967; McKenzie *et al.* 1974).

2.3. *Numerical techniques*

In the nonlinear regime solutions have to be obtained numerically. The program used was originally constructed in order to test components of a code developed for three-dimensional computations (T. B. Lennie *et al.*, in preparation) and has been designed to take particular advantage of vector computers like the Cray-1. The equations are solved by finite-difference methods, with second-order accuracy, on a grid with equal intervals in the x- and z-directions. The temperature is advanced on four interlocking meshes, using an explicit method that combines a leapfrog scheme for the nonlinear term with a Dufort–Frankel scheme for the diffusive term (McKenzie *et al.* 1974; Moore, Peckover & Weiss 1974). This 'four-colour' method generates values of T on two separate meshes at each time-step, and the stream function ψ is obtained by expanding both sides of (2.8) as finite Fourier sine series and using a combination of

fast-Fourier-transform algorithms and tridiagonal inversion techniques (Moore 1988*a*; Moore & Wallcraft 1988). The boundary conditions (2.9) are satisfied by use of a capacitance matrix (Hockney 1970). This essentially involves solving first the homogeneous Dirichlet problem corresponding to (2.8) with $\psi = \omega = 0$ on all the boundaries and then adding a linear combination of solutions, each of which has $\omega = 0$ at all interior points and at all but one of the points on the upper and lower boundaries. This combination is chosen so that the resulting stream function satisfies the boundary condition $\partial\psi/\partial z = 0$ at $z = 0, 1$. Full details of this method are given by D. R. Moore (in preparation).

The number of mesh intervals in the vertical direction N_z is of the form $N_z = p \times 2^q$, so as to facilitate the use of FFT techniques. For the runs described here N_z was varied between 8 and 160 in order to obtain adequate resolution. The number of mesh points is therefore given by λN_z^2 and the time-step Δt was kept small enough to ensure accuracy and stability. For sufficiently large Rayleigh numbers, $\Delta t \propto N_z^{-1}$ so that the total computing time varies as λN_z^3. We find that, in order to obtain an error of less than 1 % in the Nusselt number N for steady convection at high R in a layer heated from below, the mesh must have $N_z \geqslant 12N$. This corresponds to having at least 6 mesh intervals across a thermal boundary layer. Note that the boundary-layer structure is more complicated for rigid than for free boundaries and that twice as many mesh intervals are needed to ensure an accurate solution (cf. Schneck & Veronis 1967; Moore *et al.* 1974).

3. Unstable thermal boundary layers

In this section we describe the onset of time-dependent behaviour in a layer heated uniformly from below, so that $\epsilon_0 = 0$ and $T(x, 0) = 1$ (case (*a*) of table 1). Convection first sets in for rolls that are almost square in cross-section and nonlinear solutions have been obtained for finite (Schneck & Veronis 1967; Plows 1968; Clever & Busse 1974) and infinite (Busse 1967) values of σ. We studied this problem in order to check our code and calibrate its accuracy, and we have computed solutions for $1800 \leqslant R \leqslant 10^6$ with $\lambda = 1$. Our results are in close agreement with linear theory for R close to R_0 and with steady solutions obtained by Busse (1967) for $R \leqslant 3 \times 10^4$.

At $R = R_0$ two solution branches, corresponding to steady clockwise or anticlockwise motion, bifurcate from the static solution. We have obtained stable steady solutions for $R \leqslant 5 \times 10^5$; the corresponding values of N are listed in table 2 and plotted against R in figure 1(*a*). For $R \geqslant 10^4$ these results are consistent with Busse's (1967) relation

$$\frac{R}{R_c}(N-1) = 1.275\left(\frac{R}{R_c}-1\right)^{1.25} \tag{3.1}$$

but for $R \geqslant 2 \times 10^4$ a marginally better fit is given by the simple power law

$$N = 1.812\left(\frac{R}{R_c}\right)^{0.22}, \tag{3.2}$$

which is very close to the asymptotic power law of Roberts (1979).

When $\epsilon_0 = 0$ the system (2.4), (2.8)–(2.11) is invariant under the transformation

$$\psi(x, z) = \psi(\lambda - x, 1 - z), \quad T(x, z) = 1 - T(\lambda - x, 1 - z). \tag{3.3}$$

Steady solutions			Oscillatory solutions			
R	N_z	N	R	N_z	$N_{\min}$	$N_{\max}$
2.5×10^3	64	1.481	5.5×10^5	96	6.31	6.94
10^4	64	2.611	6.5×10^5	96	6.65	7.47
3×10^4	64	3.38	7.6×10^5	128	6.93	7.81
10^5	64	4.45	7.8×10^5	160	6.96	7.84
2×10^5	64	5.18	8.1×10^5	160	7.03	7.92
4×10^5	80	6.02	8.5×10^5	160	7.13	8.04
5×10^5	96	6.30	9.5×10^5	160	7.36	8.29
6×10^5	96	6.55 (unstable)	10^6	160	7.40	8.47

TABLE 2. Convection in a layer heated uniformly from below

The steady solutions on branches that bifurcate from the static solution all possess the strong Boussinesq symmetry (3.3), corresponding to point symmetry about the centre of the roll. Note that the boundary conditions at $x = 0, \lambda$ imply that the solution can be extended by assuming that it is periodic in x, with period 2λ, and imposing reflection symmetry about $x = 0$, so that $\psi(-x,z) = -\psi(x,z)$ and $T(-x, z) = T(x,z)$. Then the two solution branches bifurcating from $R = R_0$ are related by a translation λ in the x-direction.

In addition to the fundamental mode with a single roll there are higher modes with more than one roll in the box. The mode with an eigenfunction $\psi \propto \sin(m\pi x/\lambda)$, corresponding to m rolls, bifurcates from the trivial solution at $R_0^{(m)} = R_0(\lambda/m)$ and we shall only consider aspect ratios such that $R_0^{(m)} < R_0^{(m+1)}$, $m = 1, 2, 3, \ldots$. For each value of m there is a pair of solution branches with opposite senses of motion which remains distinct from pairs with different values of m. We assume that the static solution is globally stable for $R < R_0^{(1)}$, that equilibrium solutions are bounded for all finite values of R and that each pair of solution branches persists for all $R > R_0^{(m)}$. The corresponding solutions may gain or lose stability at secondary bifurcations and any two pairs of solution branches may be linked by branches of mixed solutions emerging from these bifurcations.

We have looked for secondary bifurcations from the pair of solution branches with $m = 1$. The simplest bifurcation of codimension one is a saddle-node but since we found no evidence of saddle-node bifurcations or associated hysteresis we shall ignore this possibility. The remaining generic bifurcations of codimension one are an oscillatory (Hopf) bifurcation and a transcritical stationary bifurcation (Guckenheimer & Holmes 1983); the latter may be forced by symmetries to become a pitchfork. (In simple systems like the Lorenz (1963) equations the only possibility is a Hopf bifurcation (Sparrow 1982).) What happens depends on whether the symmetry (3.3) is broken or not. If the symmetry is maintained there may be a Hopf bifurcation leading to oscillations about a steady solution with $m = 1$ or a stationary bifurcation leading to two branches of mixed solutions that are not mapped into each other when the sense of the perturbation is reversed. It does not, however, follow that the bifurcation itself must be transcritical. When the branch of mixed solutions involves perturbations of order ϵ corresponding to rolls with odd m there is a pitchfork bifurcation and any symmetry enters only at $O(\epsilon^3)$. If the symmetry (3.3) alone is broken at the bifurcation then the generic possibilities are a Hopf bifurcation or a pitchfork bifurcation leading to two steady solution branches related by the

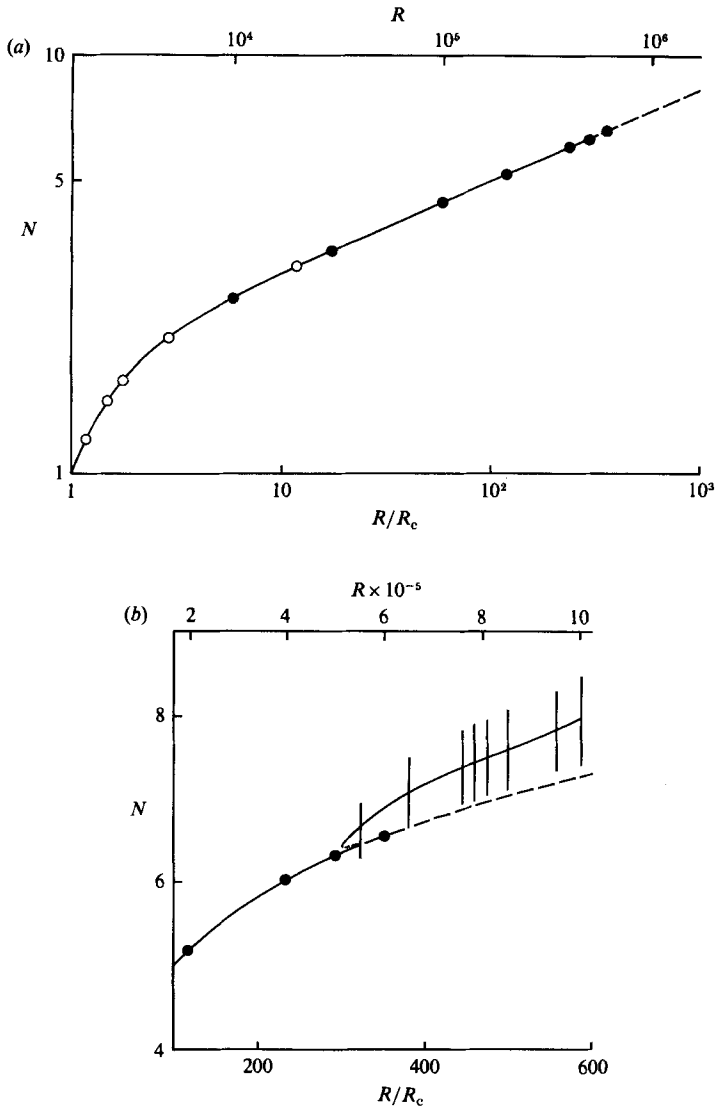

FIGURE 1. Variation of Nusselt number with Rayleigh number for convection in a layer heated from below ($\lambda = 1$). (*a*) Steady solutions: filled circles denote our results, open circles those of Busse (1967). (*b*) Branches of steady and oscillatory solutions: vertical lines indicate amplitudes of oscillations. Broken lines indicate the unstable continuation of the steady branch.

symmetry (cf. T. B. Lennie *et al.*, in preparation). Curry *et al.* (1984) located both types of Hopf bifurcation for two-dimensional convection with free boundaries and a finite Prandtl number. In this problem, however, the symmetry (3.3) is always preserved and there is only an oscillatory bifurcation.

The run with $R = 5 \times 10^5$ shows oscillations that gradually decay but at $R = 6 \times 10^5$ there are slowly growing oscillations about the steady state. Apparently there is an oscillatory (Hopf) bifurcation at $R \approx 5.5 \times 10^5$. For this value of R there are already stable finite-amplitude oscillations about the steady solution; indeed the solution for $R = 5 \times 10^5$ behaved as though the trajectory was lingering near the ghost of a large-amplitude limit cycle. It seems, therefore, that the bifurcation is

subcritical and that stable oscillations first appear at $R \approx 5.2 \times 10^5$. We find that periodic oscillations persist at least up to $R = 10^6$. The maximum and minimum values of N are listed in table 2 and the bifurcation diagram is shown in figure 1 (*b*).

It is, of course, well known that inadequate resolution may lead to spurious oscillations (Schneck & Veronis 1967) but we are confident that the oscillations we have found are genuine. We have computed solutions for $N_z = 80$, 96, 128 and 160 and the same pattern of behaviour persists as the number of mesh intervals is doubled. Moreover, the typical thickness δ of a thermal boundary layer is about one-tenth of the layer depth at $R = 5 \times 10^5$ and for $N_z = 96$ there are 9 intervals across it. This resolution is sufficiently accurate for steady solutions but as the oscillations grow more violent it becomes difficult to resolve fine structure within the boundary layers. Hence we have not sought solutions for $R > 10^6$.

Furthermore, we expect that the thermal boundary layers will become unstable for sufficiently large values of R (Howard 1966; Busse 1967; Spiegel 1971). The boundary-layer thickness $\delta \approx (2N)^{-1}$ and the local value of the Rayleigh number for the boundary layer itself,

$$\tilde{R} = \tfrac{1}{2}\delta^3 R \sim R^{0.38}, \tag{3.4}$$

increases with increasing R, from (3.2). When $\tilde{R}$ exceeds some critical value $\tilde{R}_c$ the boundary layer should become unstable to modes with wavelengths of order δ. To estimate $\tilde{R}_c$ we note that for a layer with one fixed and one free boundary $\tilde{R}_c \approx 1100$ and that R_c is further reduced for penetrative convection (cf. Moore & Weiss 1973*b*); from our results we find that $\tilde{R}_c \approx 250$. It must be emphasized that this thermal instability differs from the mechanism that produces oscillations at finite σ for convection between free boundaries. There $\tilde{R}$ remains subcritical and advection of vorticity becomes important; here only the temperature is advected by the flow.

Inspection of the solutions shows that the symmetry (3.3) is maintained in the oscillatory regime. It follows that there must be an odd number of pairs of hot and cold blobs. In our experiments three pairs circulate around the cell, giving rise to strictly periodic oscillations (once transients have died away). As fluid moves along the lower (upper) boundary a hot (cold) blob develops, with a width of order δ, and eventually breaks away from the boundary as a rising (sinking) thermal, only to be swept into the rising (sinking) plume at the edge of the cell. The blob decays as it is carried round until it returns to the boundary where it was formed, when the cycle is repeated. Meanwhile, however, two other blobs have experienced a similar development. Clearly, this process depends on the ratio of the growth time in the boundary layer to the turnover time in the cell. If this ratio is sufficiently small, blobs may break away and totally disrupt the cell. It is possible that such behaviour, preceded by further bifurcations, occurs for higher values of R in this problem. As thermals form, however, the horizontal temperature gradient is reversed and vorticity changes sign within the boundary layer. To follow such structures in detail requires a further refinement of the mesh and we have therefore concentrated on the more interesting problem of a layer heated from within, where the same mechanism leads to chaotic oscillations. In addition, we have looked at convection driven by a fixed heat flux from below (case (*b*) of table 1), where steady solutions persist at least up to $R = 3.6 \times 10^6$. Since this only corresponds to $R \approx 6 \times 10^5$ for case (*a*), the result is not surprising.

Once three-dimensional disturbances are admitted, instabilities set in at a lower Rayleigh number and rolls are only stable for $R < 22600$ (Busse 1967). Although cross-rolls are the most effective instability it is still possible to locate oscillatory

instabilities with sinusoidal variation in the y-direction (corresponding to travelling or standing waves). For finite σ this behaviour can occur with a single symmetrical pair of blobs, satisfying (3.3), or with two pairs that break the symmetry (Bolton, Busse & Clever 1986) but the case with infinite Prandtl number has not yet been investigated. In an experimental study of convection in silicone oil with $\sigma = 130$, Bergé & Dubois (1979) observed oscillatory behaviour. The box contained a single square cell, with a hot plume rising at the centre, and they showed that periodic oscillations in w were associated with the formation of a hot blob in the lower boundary layer. In a system whose planform deviated slightly from the symmetry of a square they found that oscillations appeared when $R \approx 280R_c$ but with a symmetrical cell the oscillatory bifurcation was postponed to $R \approx 420R_c$; these values agree well with our results. Moreover, as R was increased they detected period doubling followed by a transition to aperiodic (or chaotic) oscillations.

4. Quasi-periodicity and chaos

The remainder of this paper is concerned with convection in a layer heated from within. The static conducting solution given by (2.16) has a temperature $T_0 = \frac{1}{2}$ at the lower boundary so that, from (2.15), the Nusselt number $N = 2$ in the absence of convection. Similarly, the Rayleigh number as defined by (2.6) is based on a (dimensional) temperature difference ΔT that is twice the actual temperature difference across the layer. Hence it is convenient to define modified Nusselt and Rayleigh numbers

$$M = \tfrac{1}{2}N, \quad R_1 = \tfrac{1}{2}R \tag{4.1}$$

in order to facilitate comparison with other problems (cf. Roberts 1967; McKenzie *et al.* 1974).

4.1. *Fixed temperature at lower boundary*

In an experimental realization of this problem it would be possible either to keep the lower boundary at a fixed temperature T_0 or to have an insulating boundary so that there is no heat flux into the layer from below. In the former case both T_0 and R must be prescribed; if we wish to vary a single parameter we must therefore impose some arbitrary relationship between them. The natural choice, corresponding to case (*c*) of table 1, is to set T_0 equal to the value it would have for a static layer with the same (dimensioned) heating rate and no heat flux from below. This implies that $\epsilon_0 = 1$, $T_0 = \frac{1}{2}\Delta T$ in both the conducting and the convecting regime. It follows that once convection has set in some fraction of the total heat flux is supplied from below and this fraction increases with increasing R, as convection becomes more efficient.

For sufficiently large R we therefore expect to find behaviour like that described in §3 with thermal boundary layers at the upper and lower boundaries, though the symmetry (3.3) no longer holds. By analogy with those results oscillations should appear when $N \approx 6$. For $R = 4 \times 10^5$ and $\lambda = 1$ we obtain a steady solution with $N = 6.09$ but by $R = 4.4 \times 10^5$ an oscillatory bifurcation has occurred and when $R = 6 \times 10^5$ solutions seem to be aperiodic. These results suggest that internal heating promotes chaotic behaviour. It is, however, more instructive to isolate the effects of internal heating from those of heating from below by considering the configuration with an insulating lower boundary.

λ ...	0.25	0.5	0.75	1.0	1.5	2.0
R_0	55027	7236	3573	2868	2912	3504
R_{10}	27513	3618	1787	1434	1456	1752

TABLE 3. Onset of convection in a layer heated entirely from within ($\partial T/\partial z = 0$ at $z = 0$)

Steady solutions			Oscillatory solutions			
R_1	N_z	M	R_1	N_z	$M_{\min}$	$M_{\max}$
3×10^3	32	1.47	2.3×10^5	32	3.80	4.02
10^4	32	2.22	3×10^5	128	3.98	4.86
3×10^4	32	2.82				
10^5	32	3.42	3.1×10^5	128	3.8	5.0
2×10^5	32	3.82			(intermittent)	

TABLE 4. Convection in a layer heated from within ($\lambda = 1$)

4.2. *Heating entirely from within*

We have studied the transition to chaos in some detail for the more interesting case (*d*), with an insulating lower boundary. Table 3 shows the Rayleigh number $R_{10} = \frac{1}{2}R_0$ at which the pitchfork bifurcation occurs, as a function of the cell width λ (cf. Roberts 1967). Nonlinear behaviour was first investigated by Roberts (1967), using the mean-field approximation. He found that rolls were dominated by a single thermal boundary layer at $z = 1$, whose thickness $\delta \sim (Ra^2 \ln Ra^2)^{-\frac{1}{6}}$ as $R \to \infty$, while the Nusselt number $M \approx (Ra^2 \ln Ra^2)^{\frac{1}{5}}$, where $a = \pi/\lambda$. As R was increased the preferred roll width decreased but for R sufficiently large, hexagons with downward plumes at their centres were preferred to rolls. Thirlby (1970) carried out two- and three-dimensional numerical experiments with a finite Prandtl number $\sigma = 6.8$. When $R_1 = 5000$ the preferred roll width had decreased by 20% and downward hexagons were preferred for $R_1 \gtrsim 10^4$. Further computations on two-dimensional convection, with σ infinite but between free boundaries, were done by McKenzie *et al.* (1974) who found a transition from steady motion to chaotic behaviour, followed by splitting into several cells, for $R_1 \approx 7\times10^5$.

In this section we describe results obtained for rolls with square cross-section ($\lambda = 1$). Steady solutions are listed in table 4 and the modified Nusselt number M is plotted against the Rayleigh number in figure 2(*a*). Figure 3 shows isotherms, vorticity profiles and streamlines for steady convection at $R_1 = 2\times10^5$. The symmetry (3.3) no longer applies and there is a single prominent boundary layer at the top of the cell, with a cold plume descending at one side. The fluid heats up as it moves, so the hottest region lies immediately below the boundary layer and all the fluid has to approach the cool region in order to lose heat. Vorticity is generated at the edge of the sinking sheet, where $|\partial T/\partial x|$ is greatest, and at the fixed boundaries, while the maximum velocity is in the sinking slab. Since there is only one thermal boundary layer, its thickness $\delta \approx N^{-1} = (2M)^{-1}$ for large R. From figure 2(*a*) we find that

$$M \approx 1.724\left(\frac{R}{R_c}\right)^{0.16}, \tag{4.2}$$

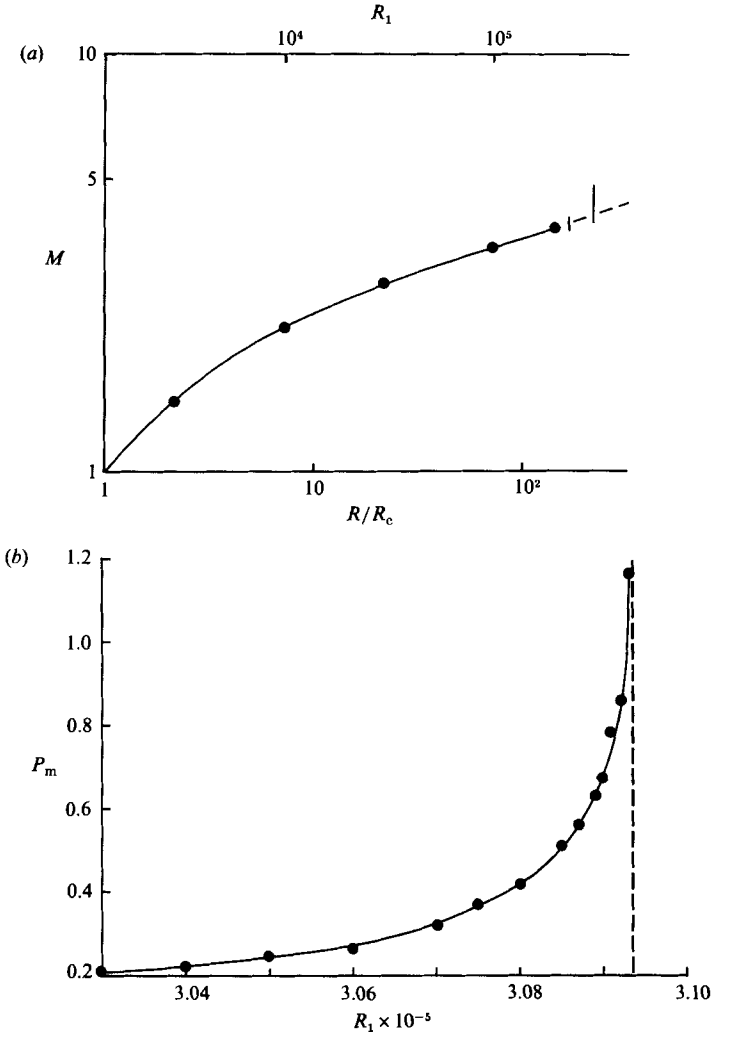

FIGURE 2. (*a*) Variation of modified Nusselt number with Rayleigh number for convection in a layer heated from within ($\lambda = 1$), showing transition from steady to oscillatory behaviour. (*b*) Quasi-periodic solutions: variation of the period of modulation P_m with Rayleigh number.

approximately, over the range $2 \times 10^4 \leqslant R_1 \leqslant 2 \times 10^5$. Thus $\delta \propto R_1^{-0.16}$, as with free boundaries (McKenzie *et al.* 1974), which is consistent with Roberts' (1967) result. Moreover, the local Rayleigh number

$$\tilde{R} = \frac{\delta^3 R_1}{M} \sim R_1^{0.36} \tag{4.3}$$

(cf. (3.4)), so we again expect that the boundary layer will become unstable as R is increased. For $R_1 = 2 \times 10^5$ we find that $\delta \approx 0.2$ and $\tilde{R} \approx 450$: so instability seems imminent. Note that, because there is only one prominent thermal boundary layer, with $M \approx 4$, adequate resolution can be obtained on a mesh with $N_z \approx 30$. Hence this problem is amenable to numerical investigation.

Around $R_1 = 2.2 \times 10^5$ there is an oscillatory (Hopf) bifurcation. The instability mechanism is the same as that discussed in §3, except that there are only cold blobs,

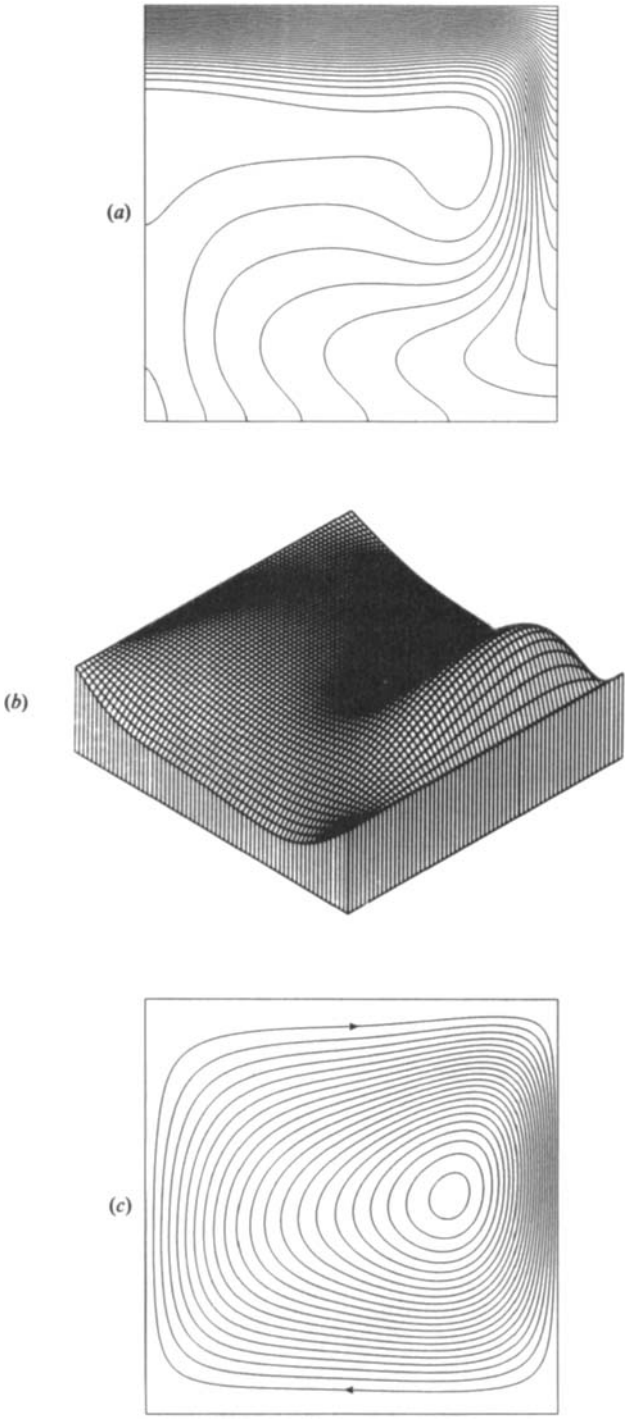

FIGURE 3. Steady convection driven by internal heating ($R_1 = 2 \times 10^5$, $\lambda = 1$). (*a*) Isotherms, (*b*) vorticity profiles and (*c*) streamlines. Motion is dominated by the sinking sheet at the right-hand boundary.

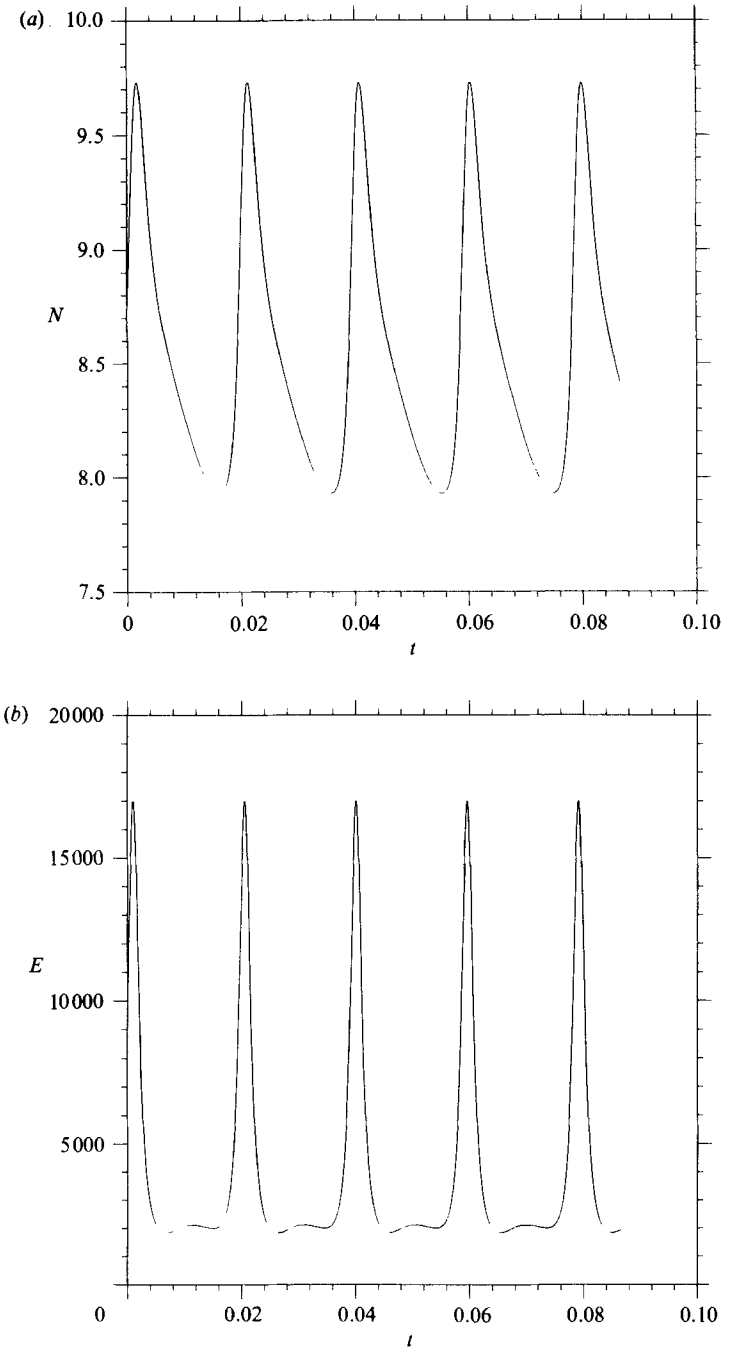

FIGURE 4(*a*, *b*). For caption see facing page.

which form in the upper boundary layer and are separated by regions that are relatively warm. For $R_1 = 2.3 \times 10^5$ the Nusselt number oscillates about the value for steady convection and by $R_1 = 3 \times 10^5$ the value of N varies by 20% during an oscillation. These periodic oscillations persist as N_z is increased from 32 to 128. In figure 4 we show N and the kinetic energy E as functions of time, together with

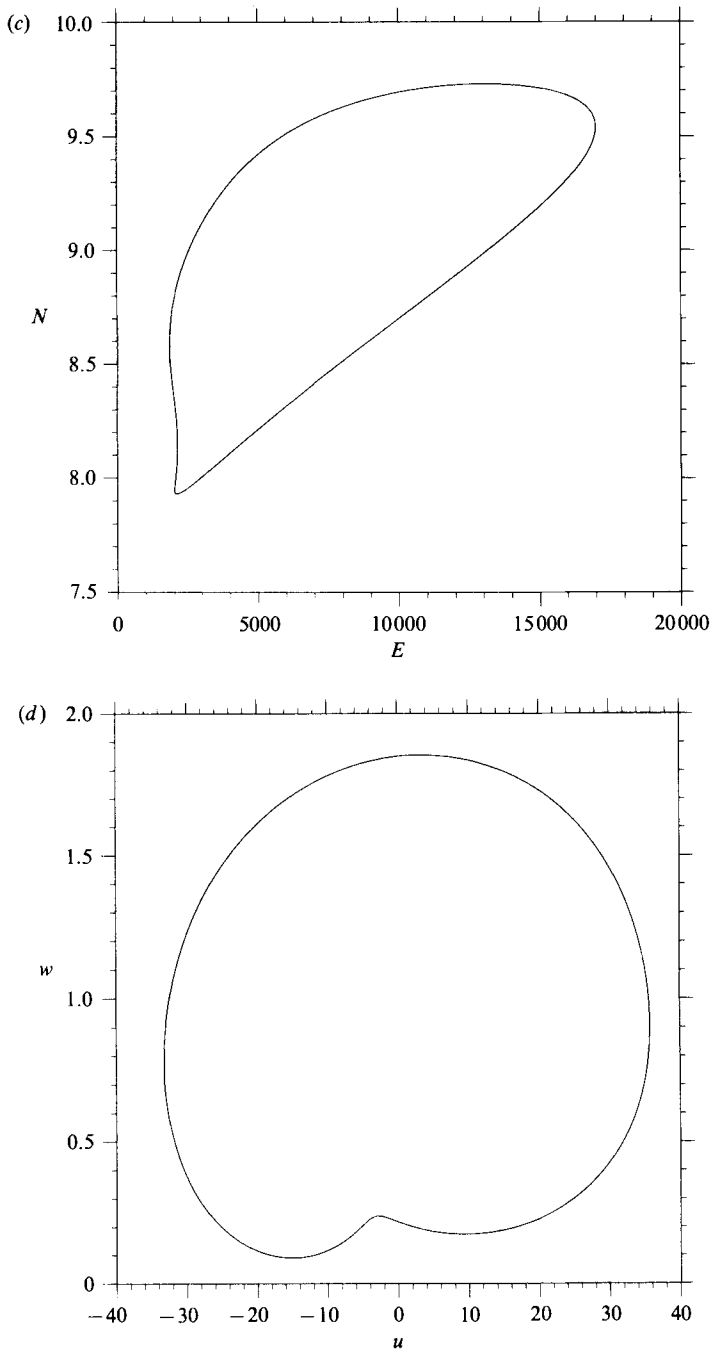

FIGURE 4. Periodic oscillations about an unstable steady solution ($R_1 = 3 \times 10^5$, $\lambda = 1$). (*a*) Variation of Nusselt number N with time; (*b*) variation of kinetic energy E with time; (*c*) projection of limit cycle onto (E, N)-phase plane; (*d*) projection of limit cycle onto the $[u(\frac{1}{2}, \frac{1}{2}, t)$–$w(\frac{1}{2}, \frac{1}{2}, t)]$-phase plane.

projections of the limit cycle onto the (E,N)-phase plane and onto the plane with coordinates given by the velocity components u and w at the midpoint of the cell. The kinetic energy has sharp maxima and flat minima, where E drops to 12% of its peak value, so the mean speed varies by a factor of three. The velocity responds instantaneously to changes in the temperature field, which are illustrated in figure 5. The first two sets of isotherms show an instability developing into a cold blob half-way across the cell; in figure 5(*c*) the blob has moved towards the sinking plume, the thermal boundary layer is distended and N (measured at the top of the cell) has reached a minimum. In figure 5(*d*) the blob is plummeting downwards, producing strong horizontal temperature gradients which generate vorticity, so that E rises to a maximum. In figure 5(*e*), the blob has reached the bottom of the cell and E has declined. Meanwhile the thermal boundary layer has contracted, so that N attains a maximum. Then, in figure 5(*f*), the next blob begins to develop and the cycle repeats again. Note that the eye of the eddy migrates upwards as the blob enters the sinking plume and then follows the blob downwards, so that the horizontal velocity u reverses at the centre of the cell.

At the end of the cycle the first cold blob has only travelled half-way round the cell and is spatially distinct from the second blob developing in the upper boundary layer. In order to understand the relationship between this spatial structure and the time-dependent motion we must bear in mind both the physics contained in the heat equation (2.4) and the nature of the oscillatory bifurcation. At the bifurcation the temperature varies harmonically with period P about its mean value at each point in an Eulerian reference frame, and the spatial structure of the oscillations is described by an appropriate complex eigenfunction. Physically, (2.4) states that temperature fluctuations are advected with the fluid subject to the effects of diffusion. The instability develops in the boundary layer and is carried into the sinking plume. As the cold blob moves across the lower part of the cell its anomalous temperature diffuses away but some remnant survives to re-enter the upper boundary layer. At the bifurcation this remnant must trigger a new instability (since the temperature fluctuation varies as $\exp(2\pi i t/P)$) which develops sufficiently rapidly during its transit across the top of the cell to survive the precipitate descent and subsequent diffusion. Thus the transition from stability to instability and the amplitude of nonlinear oscillations depend on the rate at which a blob grows in the thermal boundary layer but the period of the oscillations is determined by the time taken for a modulated thermal wave (cf. Rand 1982) to circulate around the cell, which is related to the turnover time for a typical fluid element.

As R is increased the oscillations grow in amplitude but remain strictly periodic. The cold blob that is at the base of the cell in figure 5(*e*) is smoothed out by diffusion but it can still be followed round until it re-enters the boundary layer. Close inspection of the figure shows that the circulation time for the thermal wave is twice the period of the oscillation. At any instant of time there are two cold blobs circulating round the cell; at any position in space the passage of one blob is reproduced identically as the second blob passes by after one period of the oscillation has elapsed. Since the period varies continuously the complex eigenfunction at the bifurcation must have the same structure (cf. Bolton *et al.* 1986). By analogy with studies of a ninth-order extension of the Lorenz system (M. Nagata, M. R. E. Proctor & N. O. Weiss, in preparation) we expect that the Hopf bifurcation is associated with branches of mixed solutions linking the pairs of branches with $m = 1$ and $m = 2$. Moreover, the nature of this bifurcation imposes a constraint such that the two cold blobs behave identically as they pass any position in the cell. This constraint can

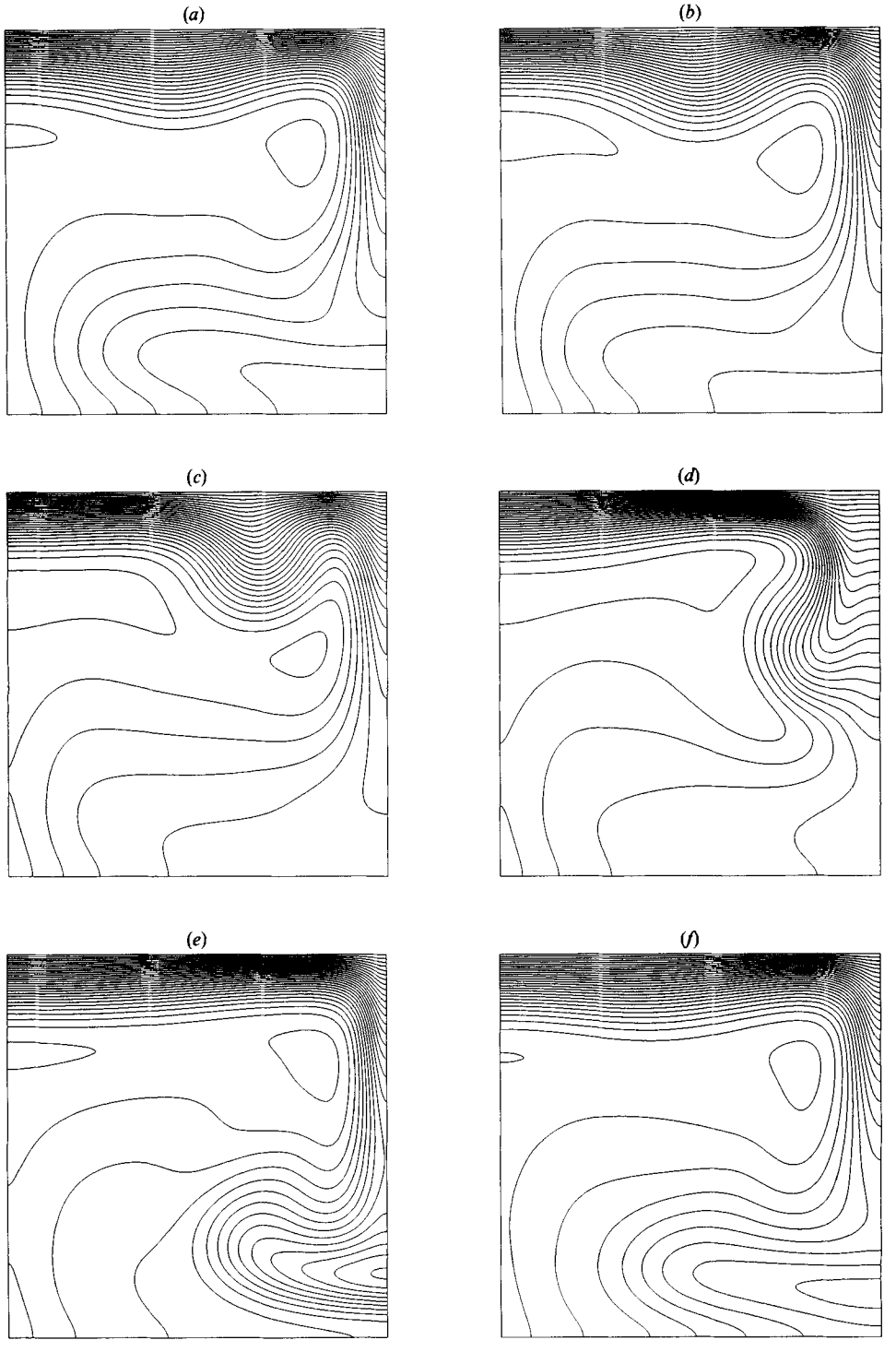

FIGURE 5. As for figure 4 but showing isotherms at equally spaced intervals during an oscillation. Note the development of a cold blob in the boundary layer which takes two periods of the oscillation to travel round the cell.

only be broken at a bifurcation. After the initial Hopf bifurcation the frequency of blob formation in the boundary layer is locked at twice the turnover frequency in the roll. As R_1 is increased these two frequencies develop differently until the nonlinear resonance can no longer be sustained. After the next bifurcation we would expect to find either period-doubling (so that each blob repeats exactly but the two are no longer identical) or quasi-periodic behaviour (with periodic modulation of the amplitude). When $\lambda = 1$ the symmetry constraint is broken by a second Hopf bifurcation but period-doubling occurs when $\lambda = 1.5$. Further bifurcations lead to complicated time-dependent behaviour; this transition is easier to follow for the case with $\lambda = 1.5$, which will be discussed in §5.

Results for $\lambda = 1$ and $R_1 = 3.1 \times 10^5$ show that one blob is more prominent than the other, so that successive peaks in N differ by about 6%. This solution is not periodic and eventually gives way to chaos. Runs at higher values of R_1 appear chaotic. In order to identify the route to chaos we have studied behaviour for $3 \times 10^5 \leqslant R \leqslant 3.1 \times 10^5$ in some detail, using a mesh with $N_z = 64$. Experience with other problems suggests that refinements of accuracy will shift bifurcations slightly without affecting their overall pattern (Knobloch *et al.* 1986). We find that there is a second Hopf bifurcation at $R_1 \approx 3.03 \times 10^5$, followed by quasi-periodic behaviour. Figure 6 shows the time sequences of N for $R_1 = 3.04 \times 10^5$, 3.08×10^5 and 3.093×10^5. Note the differences between alternate maxima or minima and the increasing period P_m of the modulation. In figure 2(*b*) this modulation period is plotted against R_1; apparently $P_m \to \infty$ as $R_1 \to R_1^{(h)} \approx 3.0935 \times 10^5$. At $R_1^{(h)}$ there is a homoclinic bifurcation and for $3.094 \times 10^5 \leqslant R_1 \leqslant 3.1 \times 10^5$ we find intermittent behaviour: episodes where the trajectory approaches a doubly periodic (P2) orbit with twice the period of the basic cycle are followed by episodes of chaos. We have not sought solutions beyond $R_1 = 3.2 \times 10^5$, where the trajectory is still chaotic.

As R_1 is decreased below $R_1^{(h)}$, the chaotic attractor persists until $R_1 = R_1^{(c)} \approx 3.071 \times 10^5$. Figure 6(*d*) shows a typical time series in the range $R_1^{(c)} < R_1 \leqslant 3.1 \times 10^5$, in which apparent order eventually gives way to chaos. As R_1 approaches $R_1^{(c)}$ from below we find that the noisy P2 behaviour is transient and solutions eventually become quasi-periodic. This behaviour can be interpreted as follows. For $2.2 \times 10^5 < R_1 < 3.03 \times 10^5$ there is a stable periodic orbit and all trajectories are attracted to a limit cycle in phase space. To investigate its stability we consider the eigenvalues μ of the return map. At $R_1 = R_1^{(o)} \approx 3.03 \times 10^5$, a pair of complex-conjugate eigenvalues cross the unit circle in the complex μ-plane, as sketched in figure 7(*a*), near $\mu = -1$ (which would correspond to period-doubling). For $R_1 > R_1^{(o)}$ these eigenvalues approach the negative real axis where they eventually merge; thereafter, one real eigenvalue moves outwards while the other decreases and eventually crosses into the unit circle at $R_1 = R_1^{(e)}$ (say). Such behaviour arises from unfolding the bifurcation of codimension 2 associated with the strong resonance at $\mu = -1$, described by Arnol'd, Takens and Bogdanov (Arnol'd 1983; Guckenheimer & Holmes 1983) which is also related to the onset of overstability in double-diffusive convection (cf. Knobloch *et al.* 1986). The corresponding bifurcation diagram is sketched in figure 7(*b*): the branch of periodic solutions undergoes an oscillatory bifurcation at $R_1^{(o)}$ and a pitchfork bifurcation at $R_1^{(e)} > R_1^{(o)}$. The latter bifurcation gives rise to a branch of unstable period-doubled (P2) solutions which could turn round at $R_1^{(c)}$ and regain stability. The branch of quasi-periodic solutions emerges at $R_1^{(o)}$ and ends on the (unstable) P2 branch at $R_1^{(h)}$, with a homoclinic bifurcation. (In general there will be horseshoes in the return map near such a homoclinic orbit.) For $R_1 > R_1^{(h)}$ we might expect to find trajectories attracted to the upper (stable) portion

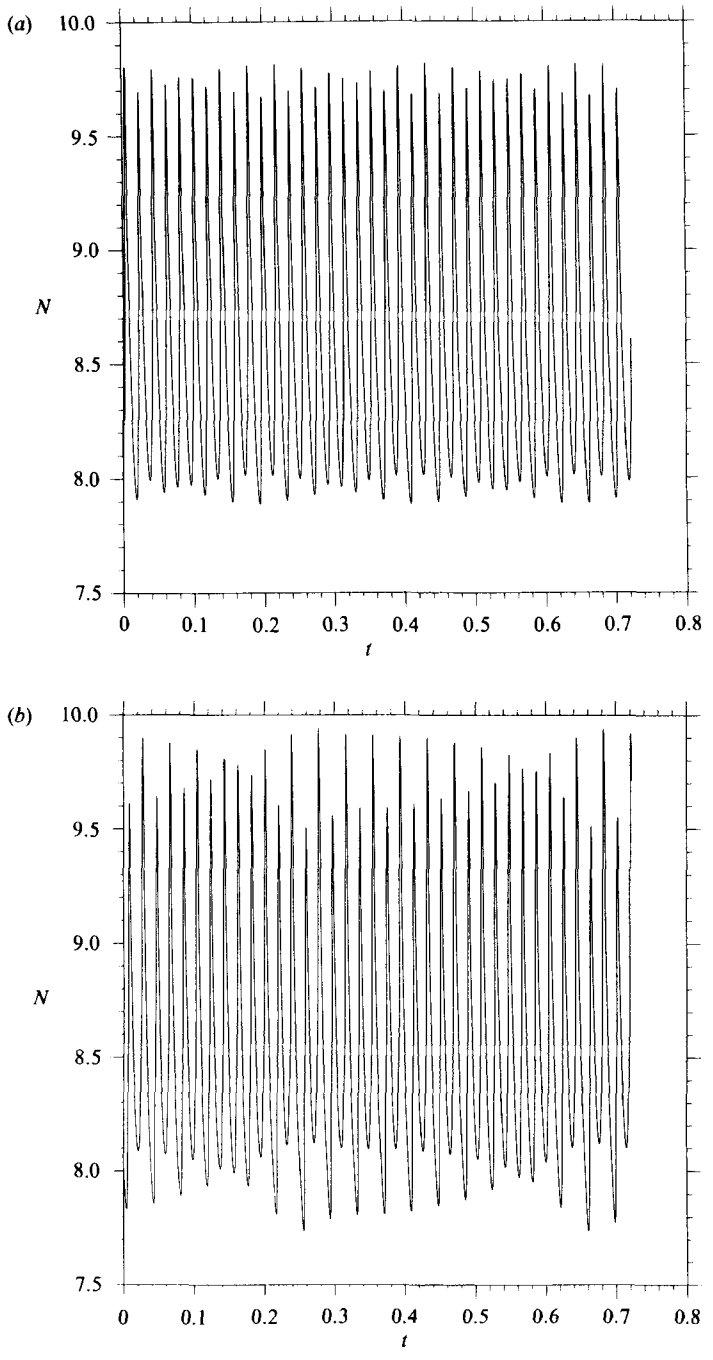

FIGURE 6(*a*, *b*). For caption see next page.

of the P2 branch. In fact they snap through into chaos and inspection of figure 6(*d*) suggests that further period-doublings occur in the process. For $t < 1.2$ there is an approximate P2 solution, which develops into P4, etc. as time increases. Apparently the P2 branch has gone through a cascade of period-doubling bifurcations before gaining stability, and a chaotic attractor appears at $R_1^{(c)}$. For $R_1^{(o)} < R_1 < R_1^{(c)}$,

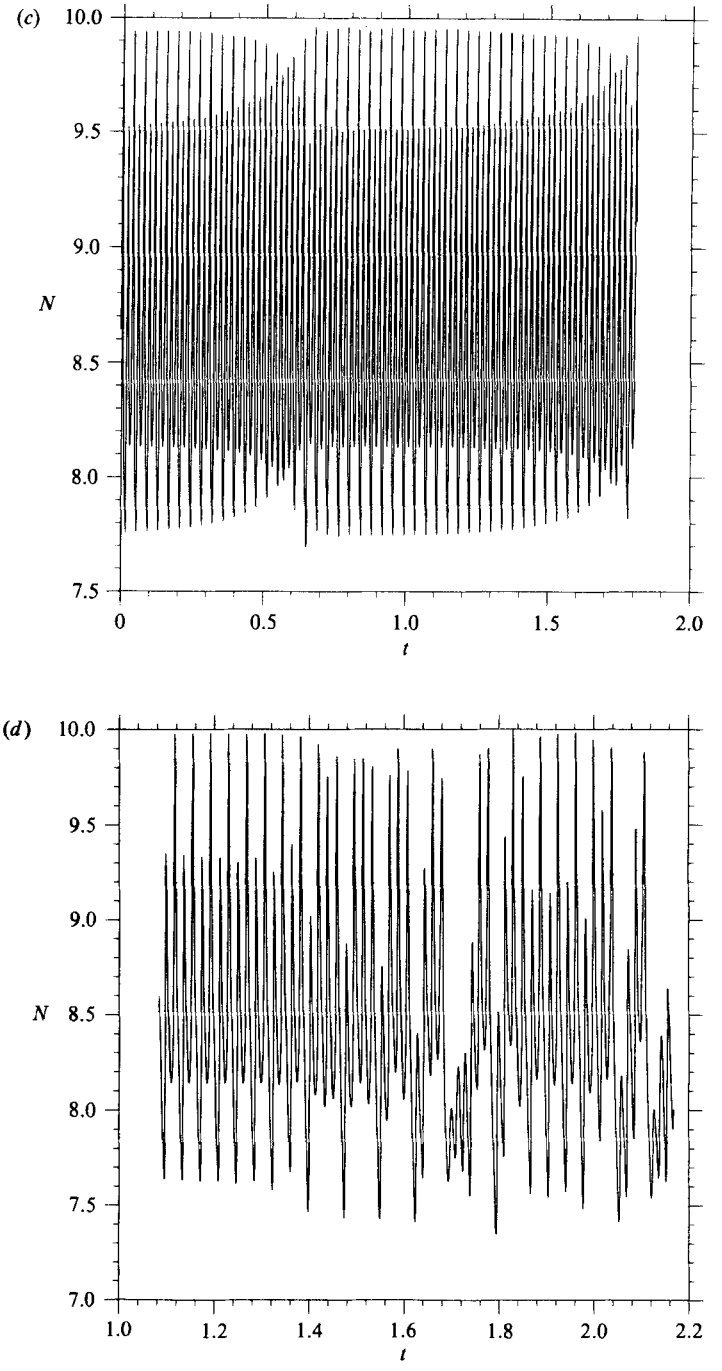

FIGURE 6. Quasi-periodicity and chaos ($\lambda = 1$). $N(t)$ for quasi-periodic (doubly periodic) solutions with (*a*) $R_1 = 3.04 \times 10^5$, (*b*) $R_1 = 3.08 \times 10^5$, (*c*) $R_1 = 3.093 \times 10^5$. (*d*) Intermittent chaos for $R_1 = 3.093 \times 10^5$. In (*a*) and (*b*) the quasi-periodic pattern, which corresponds to displacements lying on a closed curve about the unstable fixed point in the return map, is clearer at the bottom than the top of the figures.

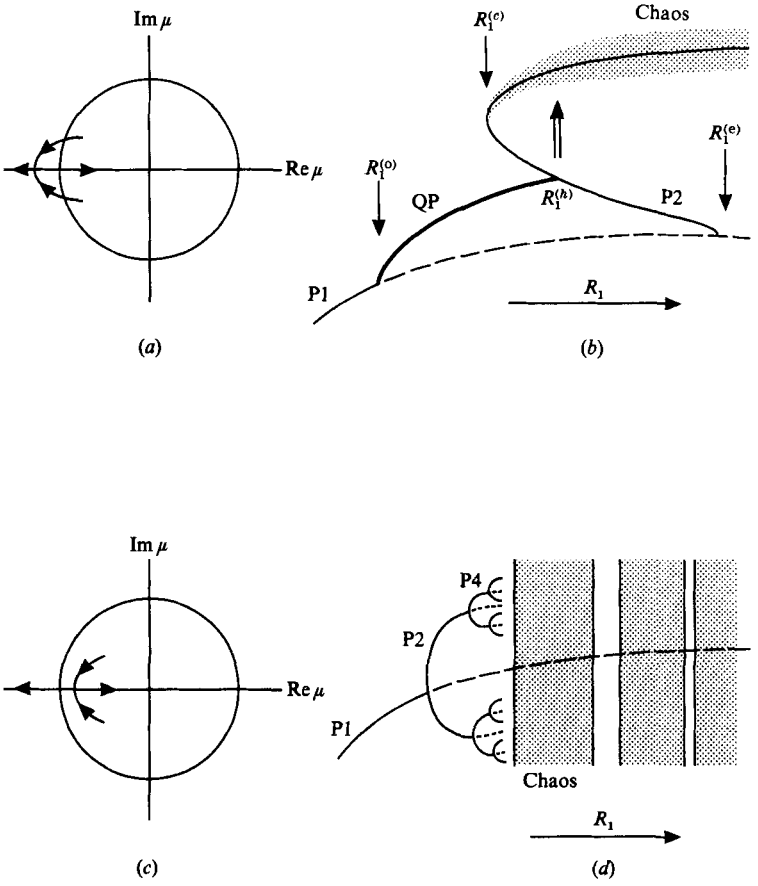

FIGURE 7. Bifurcations and transitions to chaos. (*a*) Eigenvalues crossing the unit circle in the complex μ-plane and (*b*) schematic bifurcation pattern for runs with $\lambda = 1$, showing quasi-periodicity and an abrupt transition to chaos after a homoclinic bifurcation; (*c*) and (*d*) eigenvalues and bifurcation pattern for runs with $\lambda = 1.5$, showing a period-doubling cascade leading into chaos. In the bifurcation diagrams the amplitude of the displacement in the return map is plotted against the parameter R_1.

therefore, all trajectories are attracted to a torus: for $R_1^{(c)} < R_1 < R_1^{(h)}$, either trajectories are attracted to the torus or they become chaotic. For $R_1 > R_1^{(h)}$ the only attractor is chaotic. For R_1 near to $R_1^{(h)}$, however, trajectories may approach the stable manifold of the P2 branch, so that they appear to be periodic for a finite time and then escape to undergo a burst of chaos before being reinjected into the neighbourhood of the P2 orbit. This form of intermittency differs in detail from those described by Pomeau & Manneville (1980).

We have described here a general process that leads from a steady state to chaos after two Hopf bifurcations and a homoclinic bifurcation. Such transitions have been observed in experiments (cf. figure 12 of Libchaber, Fauve & Laroche 1983). We must emphasize, however, that the underlying route to chaos is through a cascade of (unobservable) period-doubling bifurcations. In other systems we may expect to find what has eluded us here, namely a sequence of solutions with period $2, 4, \ldots$ on the stable portion of the P2 branch. Moreover, diligent search should reveal intervals in R_1 where periodic solutions interrupt the chaos, as we shall see in the next section.

R_1	Solution	R_1	Solution	R_1	Solution
2×10^4	S	1.08×10^5	P4	4×10^5	P1
4×10^4	S	1.085×10^5	P4	5×10^5	P1
6×10^4	S	1.09×10^5	P8	6×10^5	P1
8×10^4	P1	1.1×10^5	C	7×10^5	P2
9×10^4	P1	1.2×10^5	C	8×10^5	P2
9.5×10^4	P1	1.3×10^5	SP8	9×10^5	P2
9.7×10^4	P1	1.4×10^5	C	10^6	QP
9.8×10^4	P2	1.6×10^5	P4	1.2×10^6	C
10^5	P2	2×10^5	P1	1.4×10^6	C
1.06×10^5	P2	3×10^5	QP		(2 cells)

TABLE 5. Convection in a layer heated from within ($\lambda = 1.5$, $N_z = 64$)

5. Bifurcations and changing spatial structures

Convection driven by internal heating results in the formation of a cold boundary layer. We have seen that, in rolls with square cross-section, cold blobs may form and detach themselves from this layer when the Rayleigh number is sufficiently large. This instability is associated with a preference for narrower convection cells and we expect it to develop at lower values of R_1 if $\lambda > 1$: the wider the box, the thicker the boundary layer is when it breaks up, so that adequate resolution can be obtained with a relatively coarse mesh. The consequent reduction in computing time (which varies as λN_z^3) makes it feasible to investigate this process systematically. In this section we shall explore nonlinear time-dependent behaviour in rolls with $\lambda = 1.5$, keeping $N_z = 64$.

Table 5 lists the types of solution we have found. For $6\times10^4 \geqslant R_1 \geqslant R_{10}$ we obtain steady solutions (denoted by S in the table). As expected, convection is less efficient than it is with square rolls: at $R_1 = 6\times10^4$, the modified Nusselt number $M \approx 3.02$, about 5% less than the value derived from figure 2(*a*). There is an oscillatory bifurcation at $R_1 \approx 7\times10^4$ (about one-third of the corresponding value for $\lambda = 1$) when $\delta \approx 0.25$ and, from (4.3), $\tilde{R} \approx 360$. In a wider cell, a disturbance in the thermal boundary layer has more time to develop before it is swept into a sinking sheet, and so the instability sets in at a lower value of R_1. Since a new blob can develop as soon as the thermal boundary layer has recovered from its predecessor, there are likely to be several cold blobs circulating round the cell. In our numerical experiments there are always two. To describe what happens we must distinguish between three time intervals: the cycle period τ_c is the mean interval between identical phases in the formation of successive blobs; the turnover time is the time taken for a typical fluid element to circulate around the cell; and P is the period of a periodic solution. If $P = n\tau_c$, so that every nth blob behaves identically, the solution is said to be of type Pn (or, loosely, of period n). Now there is only one bifurcation of codimension one that leads to oscillations about a steady state, and that is a Hopf bifurcation. Near the bifurcation point disturbances must vary sinusoidally, although the eigenfunctions represent two spatially separated blobs. Hence the solutions are of type P1 and their period is half the turnover time. Blobs that are physically distinct are constrained to behave identically and this symmetry can only be broken by a further bifurcation.

The solutions of type P1 are similar to those for $\lambda = 1$ (cf. figures 4 and 5). At

$R_1 = 9.5 \times 10^4$ we find that $3.25 \leqslant M \leqslant 3.60$, a variation of 10%. Cold blobs begin to detach themselves from the boundary layer before they reach the sinking plume and the peaks in kinetic energy are less sharp than for $\lambda = 1$ (the fraction of the period for which E is greater than half its maximum value has increased from 13% to 33%). At $R_1 \approx 9.8 \times 10^4$ there is a supercritical pitchfork bifurcation which breaks the symmetry between the spatially separated blobs. The period doubles and becomes equal to the turnover time. At the bifurcation point a single real eigenvalue of the return map crosses the unit circle at $\mu = -1$, as sketched in figure 7(*c*); apparently the conjugate eigenvalues merge inside rather than outside the circle $|\mu| = 1$. The corresponding bifurcation diagram is sketched in figure 7(*d*). Evidently there is a bifurcation of codimension two with a double eigenvalue at $\mu = -1$ for some λ_0, $1 < \lambda_0 < 1.5$ (Arnol'd 1983; Guckenheimer & Holmes 1983). Note, however, that the P2 branch bifurcates to the left in figure 7(*a*) and to the right in figure 7(*d*) so that increasing λ from 1 to 1.5 apparently also allows a transition from a P2 branch with a turning point, to one that is monotonic (cf. figure 2 of Knobloch, Weiss & Da Costa 1981). By varying the lower boundary condition as well as λ it might be possible to locate a bifurcation of codimension three.

What happens physically at the period-doubling bifurcation is quite clear. One of the two blobs becomes more prominent; as it sinks the cold plume swells and kinetic energy increases. The other blob is swept more rapidly across the top and so has less time to develop. Thus the first blob maintains its advantage. It is less obvious why the transition from solutions of type P1 to type P2 should proceed via quasi-periodicity for $\lambda = 1$ and by period-doubling for $\lambda = 1.5$. The patterns in figure 7(*a* and *c*) are equally plausible and we conjecture that the transition from one to the other is caused by changes in the effect of diffusion as the aspect ratio is increased.

For $9.8 \times 10^4 \leqslant R_1 \leqslant 1.06 \times 10^5$ we find stable oscillations of type P2. Figure 8(*a*) shows the Nusselt number N as a function of time for $R_1 = 1.06 \times 10^5$ and it is apparent that the period $P = 2\tau_c$. The corresponding trajectory in phase space is a closed curve and figure 8(*b*) shows this limit cycle projected onto the (E, N)-plane. Note the distinction between alternative cycles, with a sharper rise for the more prominent cycles. At $R_1 \approx 1.07 \times 10^5$ there is a period-doubling bifurcation of the type familiar from studies of low-order systems. In figure 8(*c* and *d*) N and E are plotted against time for the P4 solution at $R_1 = 1.08 \times 10^5$ and the corresponding limit cycle is illustrated in figure 8(*e*). The two lobes of the P2 solution have split in such a way that three maxima in N lie close together. Figure 9 shows the variation of the temperature field during an interval of $0.4P$ which covers the formation of the smallest (second) and the largest (third) maxima in figure 8(*c* and *d*). The small blob enters the sinking plume smoothly but the larger blob produces a major distortion before it is carried to the side and generates velocities that are 10% greater. The next period-doubling bifurcation, at $R_1 \approx 1.087 \times 10^5$, is followed by solutions of type P8, with a further splitting, as shown in figure 8(*f*) for $R_1 = 1.09 \times 10^5$. This is apparently part of a period-doubling cascade which leads to temporal chaos. At $R_1 = 1.1 \times 10^5$ the solution is aperiodic, though there is still a tendency for cycles to alternate in amplitude. Both the transition to chaos and behaviour in the chaotic regime (denoted by C in table 5) are consistent with the properties of one-dimensional maps (cf. Knobloch *et al.* 1986). In particular we expect to find intervals in R_1 where periodic solutions appear, followed by period-doubling cascades and chaos. We have not searched for such windows but at $R_1 = 1.3 \times 10^5$ there is a semiperiodic (SP)

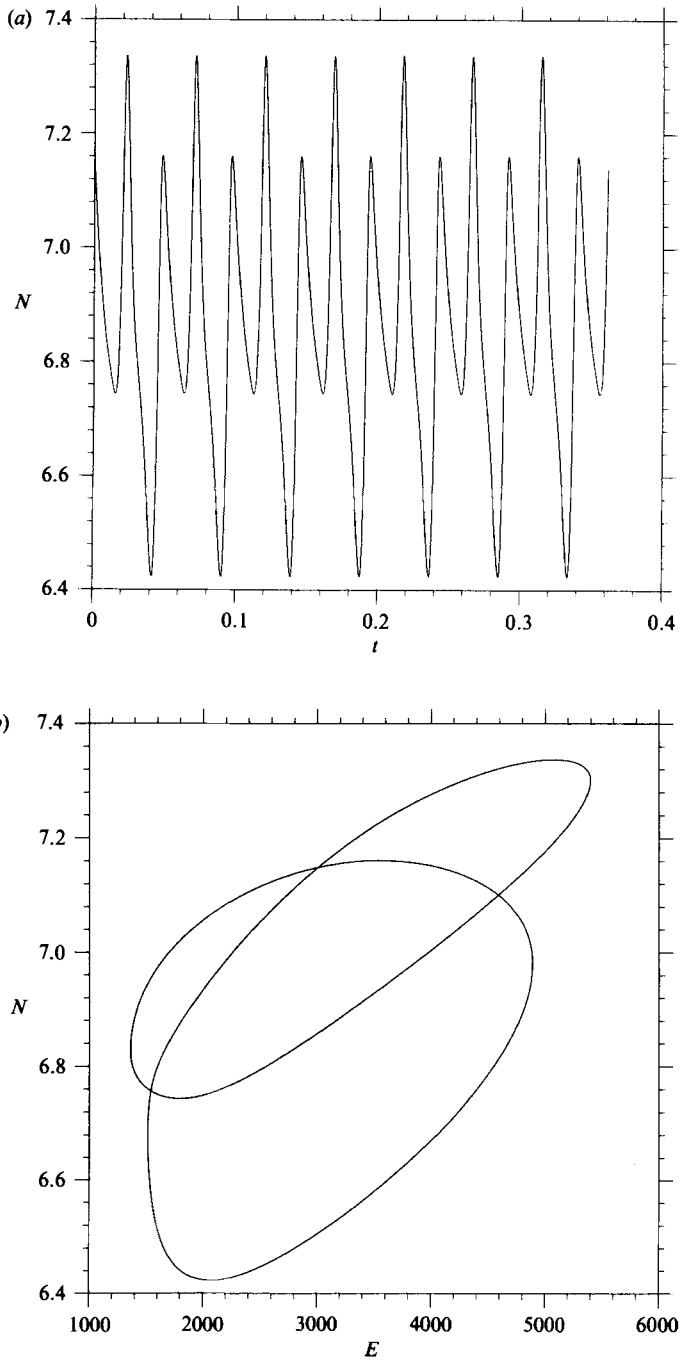

FIGURE 8(a, b). For caption see page 72.

solution apparently associated with a window of period 8. The periodic windows can be interpreted physically as resonances between the mean cycle period and the turnover time.

Chaotic behaviour does not persist, for we find a P4 solution at $R_1 = 1.6 \times 10^5$ and by $R_1 = 2 \times 10^5$ the solution is of type P1. Apparently there is an inverse cascade of

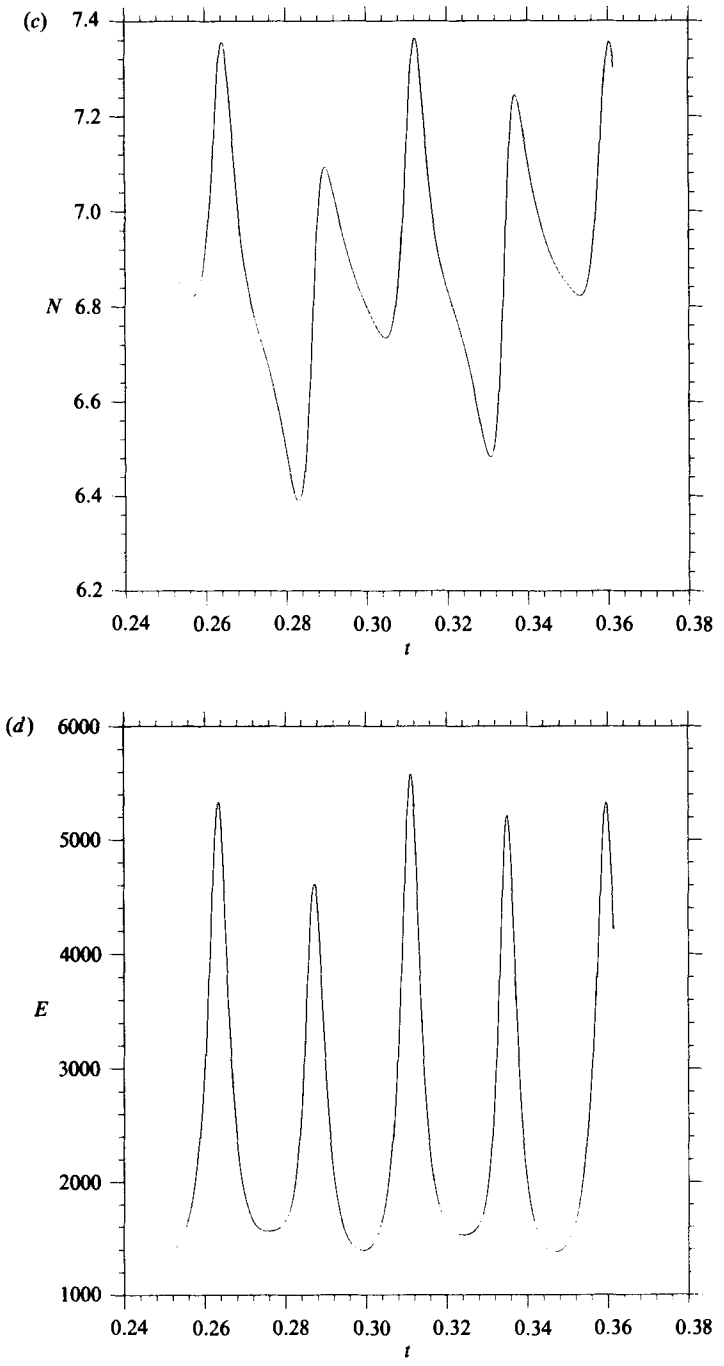

FIGURE 8(*c*, *d*). For caption see page 72.

bifurcations and chaos occurs within a 'bubble', as found for thermosolutal convection (Knobloch *et al.* 1986). As R_1 increases, however, the falling blobs develop a different spatial structure and the bifurcation sequence becomes more complicated than that of a third- or fifth-order system. Figure 10 illustrates the development of the largest blob when $R_1 = 1.6 \times 10^5$. Comparison with figure 9 shows that the blob

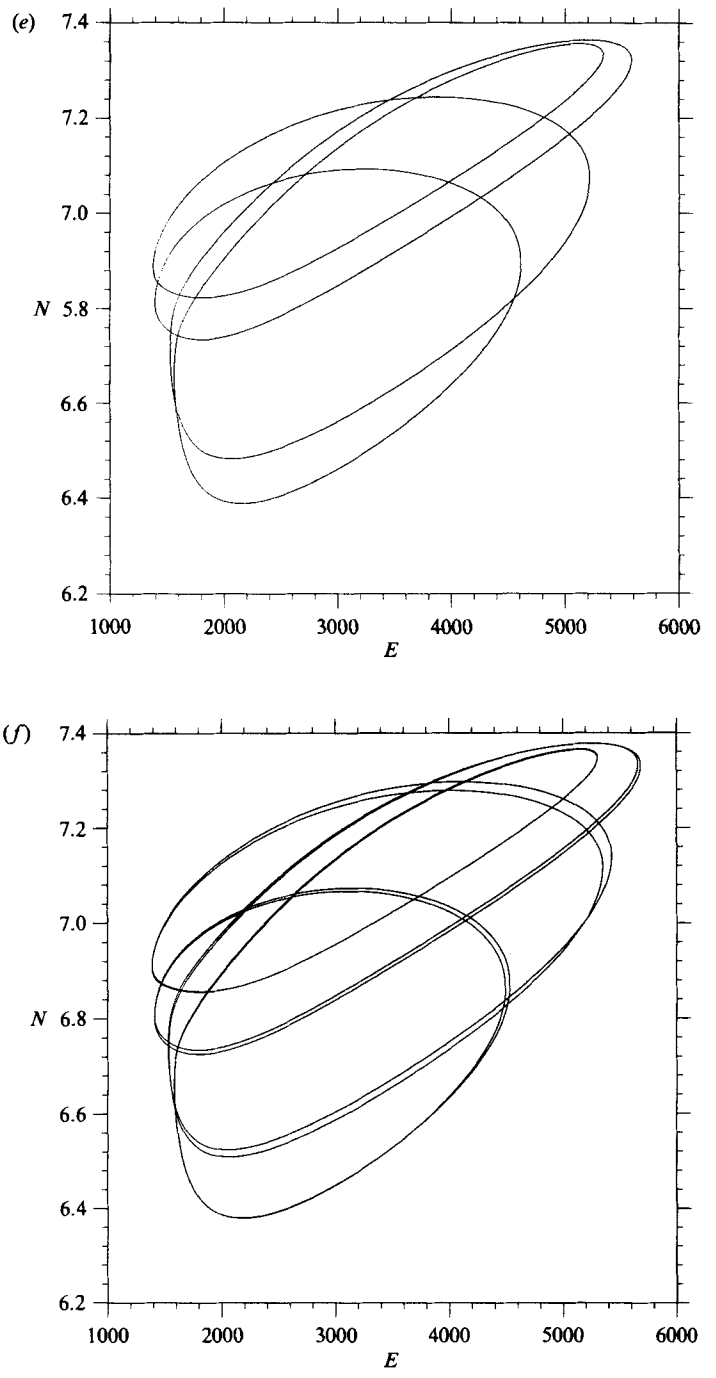

FIGURE 8. Period-doubling and chaos ($\lambda = 1.5$). (*a*) $N(t)$ and (*b*) limit cycle in (E, N)-phase plane for P2 solution with $R_1 = 1.06 \times 10^5$. (*c*) $N(t)$, (*d*) $E(t)$ and (*e*) limit cycle for P4 solution with $R_1 = 1.08 \times 10^5$. (*f*) Limit cycle for P8 solution with $R_1 = 1.09 \times 10^5$.

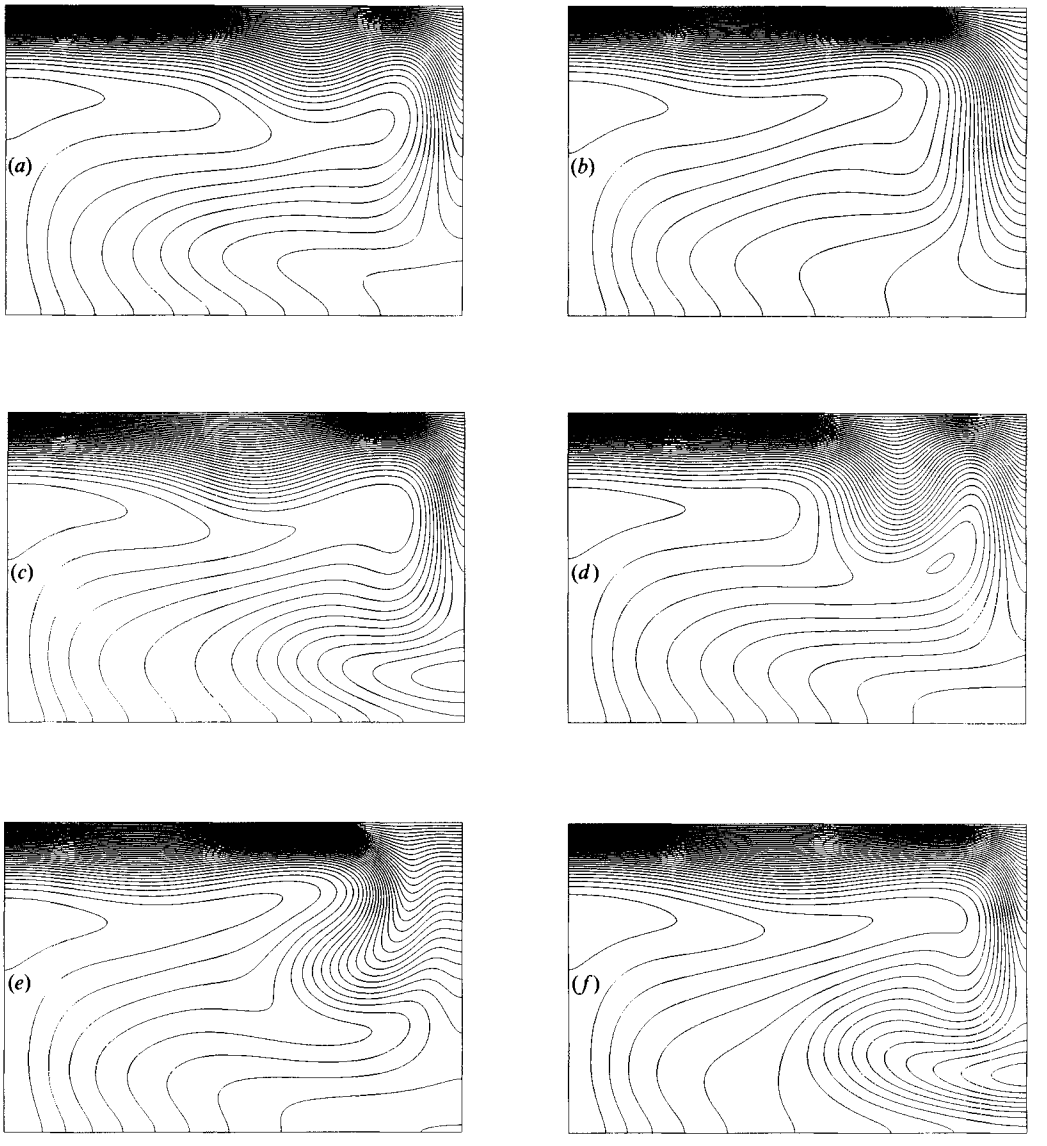

FIGURE 9. Development of non-trivial spatial structure. Isotherms at equally spaced intervals covering part of the period of the P4 solution at $R_1 = 1.08 \times 10^5$. Note the difference between successive cold blobs.

has detached itself before being swept into the sinking plume, with consequent modifications to the flow.

We have not attempted to identify all subsequent bifurcations; experience with other problems suggests that such details are intricate and may be sensitive to the limited resolution of the mesh within the blobs themselves. There are, however, periodic, quasi-periodic (QP) and chaotic regimes, as shown in table 5. At $R_1 = 4 \times 10^5$ there is a P1 solution with a permanent plume at $x = \lambda$ (say) modulated periodically by a blob that develops and plunges separately downwards at $x \approx 0.75\lambda$, as shown in figure 11. Once again there are two cold regions that are spatially separated, so that the next blob develops as the first one sinks. Once again this

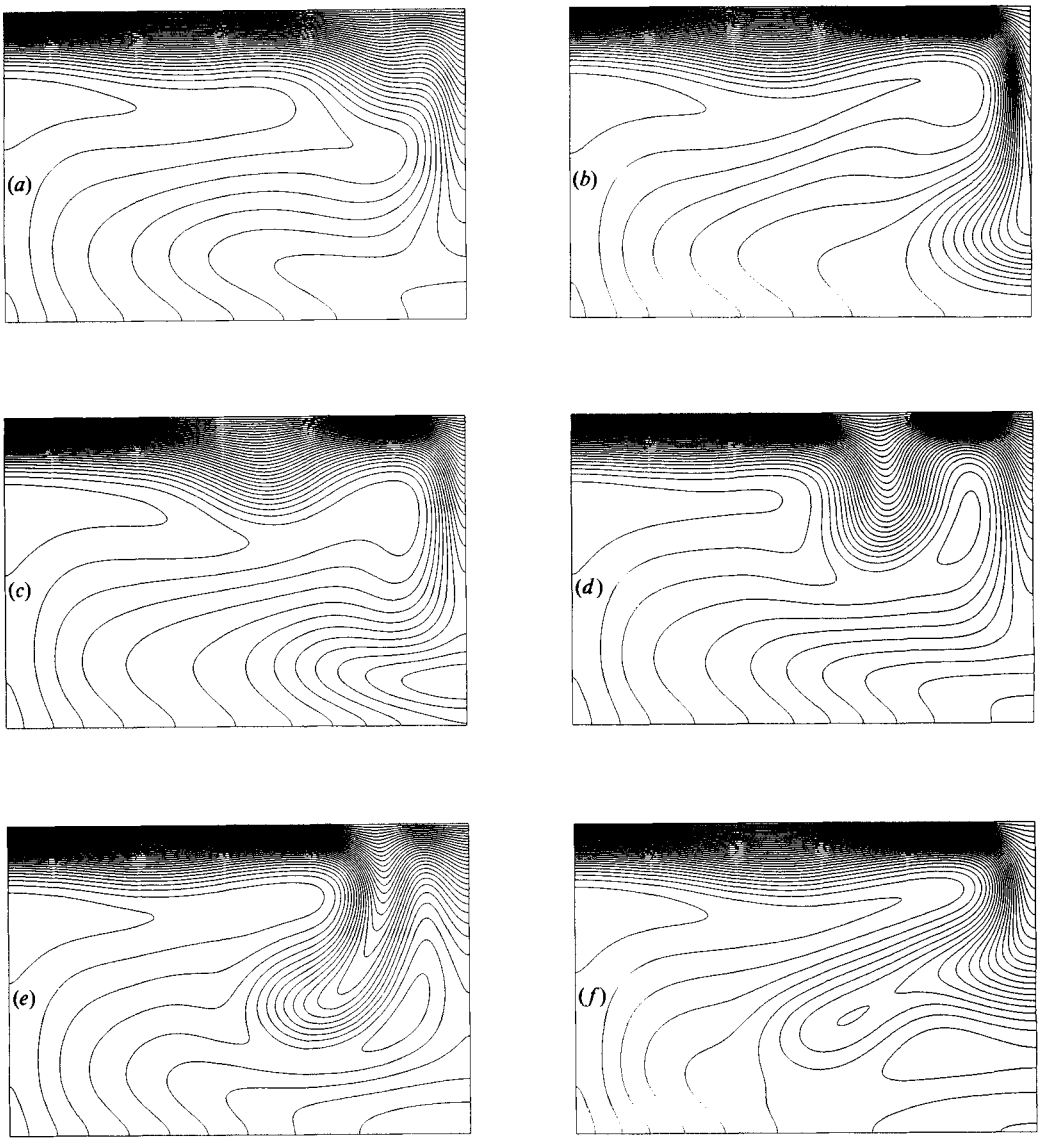

FIGURE 10. Detachment from the boundary layer. Isotherms at equally spaced intervals covering part of the period of the P4 solution at $R_1 = 1.6 \times 10^5$, after the return from chaos.

symmetry is broken at a bifurcation around $R_1 \approx 6.5 \times 10^5$. As R_1 is increased, cold blobs detach themselves and sink closer to the middle of the cell. Figure 12 shows both isotherms and streamlines as one blob forms, at $x \approx 0.6\lambda$, in the P2 solution at $R_1 = 7 \times 10^5$: the new plume has almost split the cell.

Our solutions were obtained by increasing R_1 and using results for a lower Rayleigh number to provide initial conditions. At $R_1 = 10^6$ the P2 solution became quasi-periodic and by $R_1 = 1.2 \times 10^6$ behaviour was chaotic. A single fixed plume was anchored at $x = \lambda$, while cold blobs fell irregularly near the centre of the cell for as long as the calculation was pursued; the Nusselt number varied in the range $11.5 < N < 13.3$. At $R_1 = 1.4 \times 10^6$ the solution was still chaotic but after a major convulsion, when N rose to 16, there were two plumes, anchored permanently at

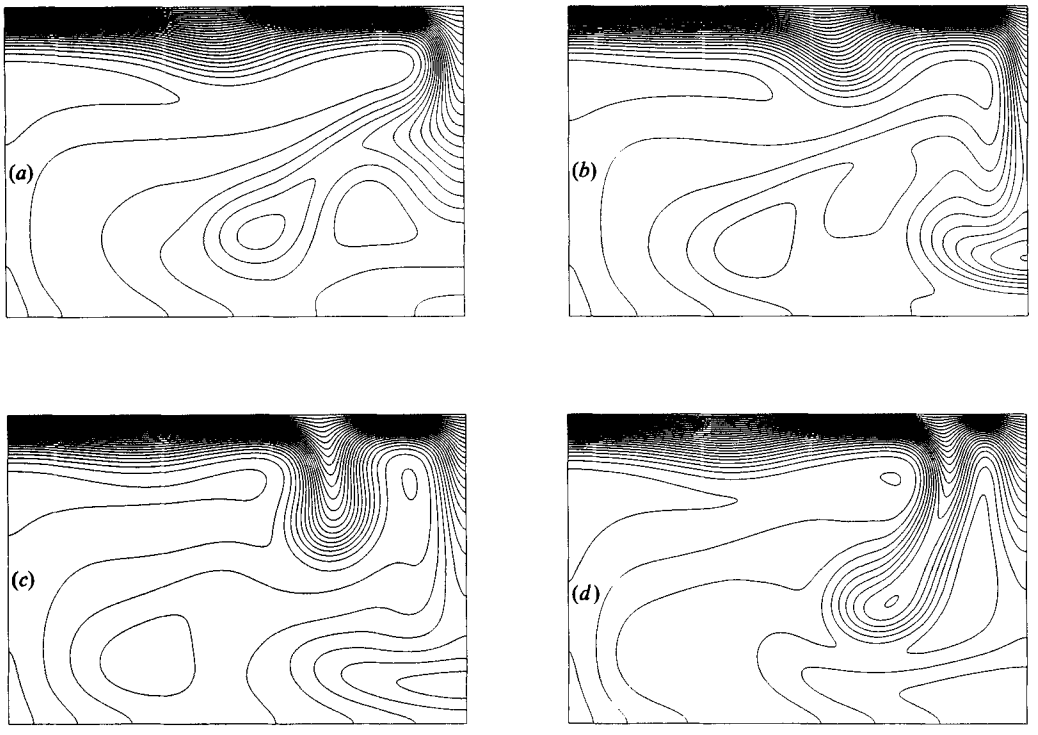

FIGURE 11. Formation of a detached blob. Isotherms at equally spaced intervals covering the P1 cycle with $R_1 = 4 \times 10^5$.

$x = 0, \lambda$. Between them, blobs formed and detached themselves from the boundary layer aperiodically. Similar behaviour was found at $R_1 = 1.6 \times 10^6$.

Viewed as a whole, these numerical experiments cover a transition from steady convection with a single roll in the box of width $\lambda = 1.5$ to unsteady convection with two rolls in the box. Much of the complicated time-dependent behaviour is associated with a change in spatial symmetry. Owing to the presence of fixed lateral boundaries the transition from one to two cells is not simple. In particular, there seem to be two distinct phases, the first involving period-doubling and chaos for $R_1 \sim 10^5$ and the second involving quasi-periodicity and chaos around $R_1 \sim 10^6$. In order to interpret these results we need to consider convection in boxes that contain several rolls.

6. Multiple rolls

In a box of width λ, subject to the boundary conditions (2.9) and (2.10), the static solution becomes unstable to perturbations of the form $\psi \propto \sin(m\pi x/\lambda)$, $m = 1, 2, 3, \ldots$, for $R > R_0^{(m)}$. Two branches of steady solutions bifurcate from the trivial solution at each point $R = R_0^{(m)}$, corresponding to nonlinear convection in rolls of width $l = \lambda/m$. The two branches correspond to different signs of ψ and are related by a symmetry. For m odd, one branch (m^+) has a cold sinking sheet at $x = \lambda$, while the other (m^-) has a sinking sheet at $x = 0$; the two branches are related by the symmetry $x \to \lambda - x$. For m even, one branch (m^+) has a sinking sheet at $x = \frac{1}{2}\lambda$, while the other (m^-) has sinking sheets at $x = 0, \lambda$. Figure 13 shows isotherms and streamlines for solutions on the 2^+ and 2^- branches with $\lambda = 1.5$. The two branches

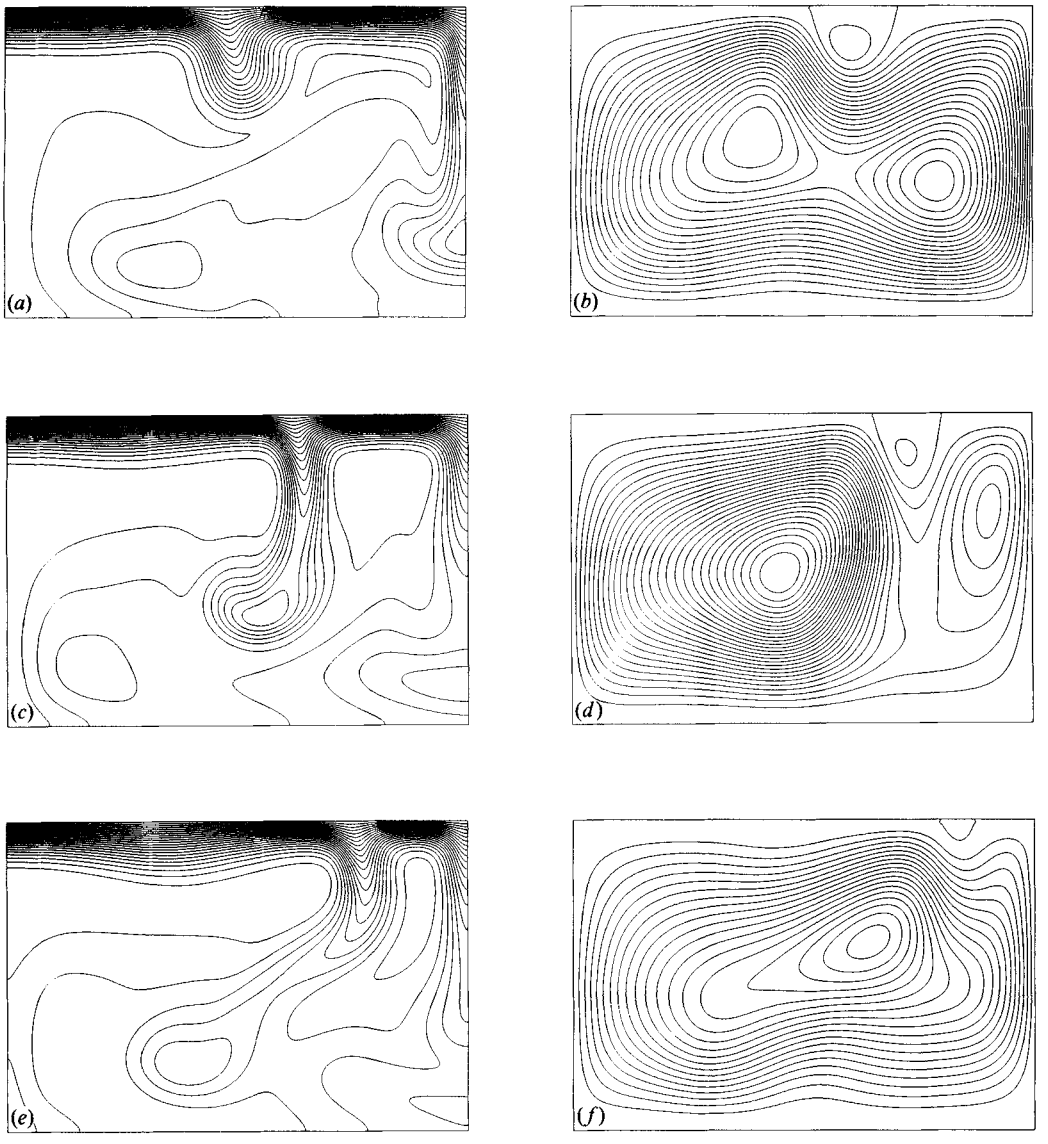

FIGURE 12. Distortion of the flow by sinking blobs. Isotherms and streamlines at equally spaced intervals covering part of the period of the P2 solution at $R_1 = 7 \times 10^5$.

are related by the symmetry $x \to x - \frac{1}{2}\lambda$ and the assumption that ψ is periodic in x. The steady solutions along the m^+ and m^- branches transform into each other under the symmetries.

We are concerned with transitions from one solution branch to another. For R sufficiently large we expect any branch of steady solutions to become unstable. New branches bifurcating from it may bifurcate themselves and eventually make a connection to some other steady branch. The stability properties of the m^+ and m^- branches are identical if m is odd but not if m is even. Then we expect the m^- solutions to be relatively more stable, since sinking sheets cannot so readily be displaced from the lateral boundaries of the box.

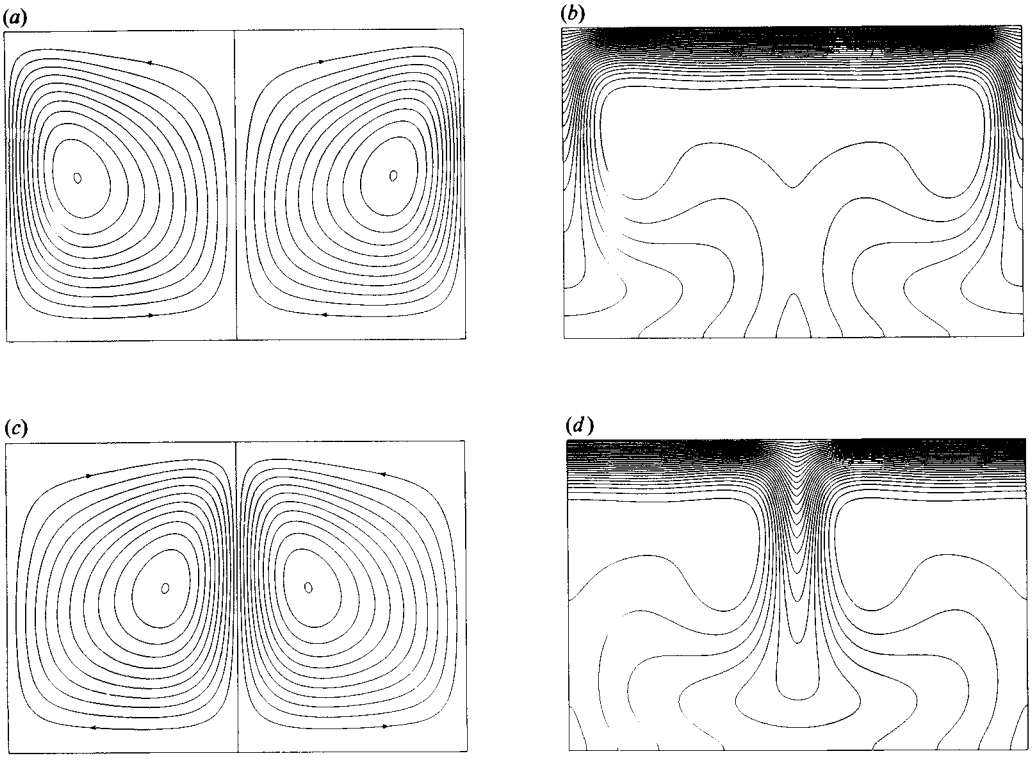

FIGURE 13. Steady convection with two rolls in a box ($R = 3.1 \times 10^5$, $\lambda = 1.5$, $m = 2$). (*a*) Streamlines and (*b*) isotherms for the 2^- solution; (*c*) and (*d*) the same for the 2^+ solution.

Solutions with $l = 1, 1.5$ and $m = 1$ have already been studied in §§4 and 5, and we have also experimented with $\lambda = 0.5, 0.75$, keeping $N_z = 64$. The relevant values of R_0 are listed in table 3. We first consider solutions with $l = 0.5$. When $m = 1$ the steady branches remain stable at least up to $R_1 = 10^6$; at $R_1 = 3.1 \times 10^5$ the value of M is 10% higher than for the (unstable) steady solution with $l = 1$, and at $R_1 = 10^6$, $M \approx 6.0$. Solutions with $m = 2$ and $\lambda = 1$ show more variety. The 2^- branch is stable at least up to $R_1 = 5.1 \times 10^5$ but the 2^+ branch is already unstable when $R_1 = 3.1 \times 10^5$. The instability violates the symmetry of the 2^+ solution about the plane $x = 0.5$ and therefore develops slowly from the rounding error until it attains a significant amplitude. Then the central plume is rapidly displaced towards one of the lateral boundaries and there is a transition to a solution with $m = 1$, which itself becomes unstable, yielding intermittent solutions of the type discussed in §4. An experiment with $m = 3$ and $\lambda = 1.5$ showed similar behaviour at $R_1 = 3.1 \times 10^5$. The sinking sheet at $x = 1.5$ remained fixed while the sheet at $x = 0.5$ eventually migrated to the boundary at $x = 0$, giving a steady 2^- solution. As a result of this transition the Nusselt number dropped by 9%.

Next we consider rolls with $l = 0.75$. When $m = 1$ solutions remain steady at least until $R_1 = 5.1 \times 10^5$. With $m = 2$ and $\lambda = 1.5$ the two branches behave differently. We first consider the 2^- branch. Stable steady solutions were obtained up to $R_1 = 5.1 \times 10^5$. Figure 13(*a* and *b*) shows streamlines and isotherms for the solution at $R_1 = 3.1 \times 10^5$. At $R_1 = 9.1 \times 10^5$ there was a slow transition to chaotic behaviour, as shown by the variation of N with time in figure 14(*a*). The final state resembles that found after the transition from $l = 1.5$ to $l = 0.75$ at $R_1 = 1.4 \times 10^6$ (cf. §5). Similar

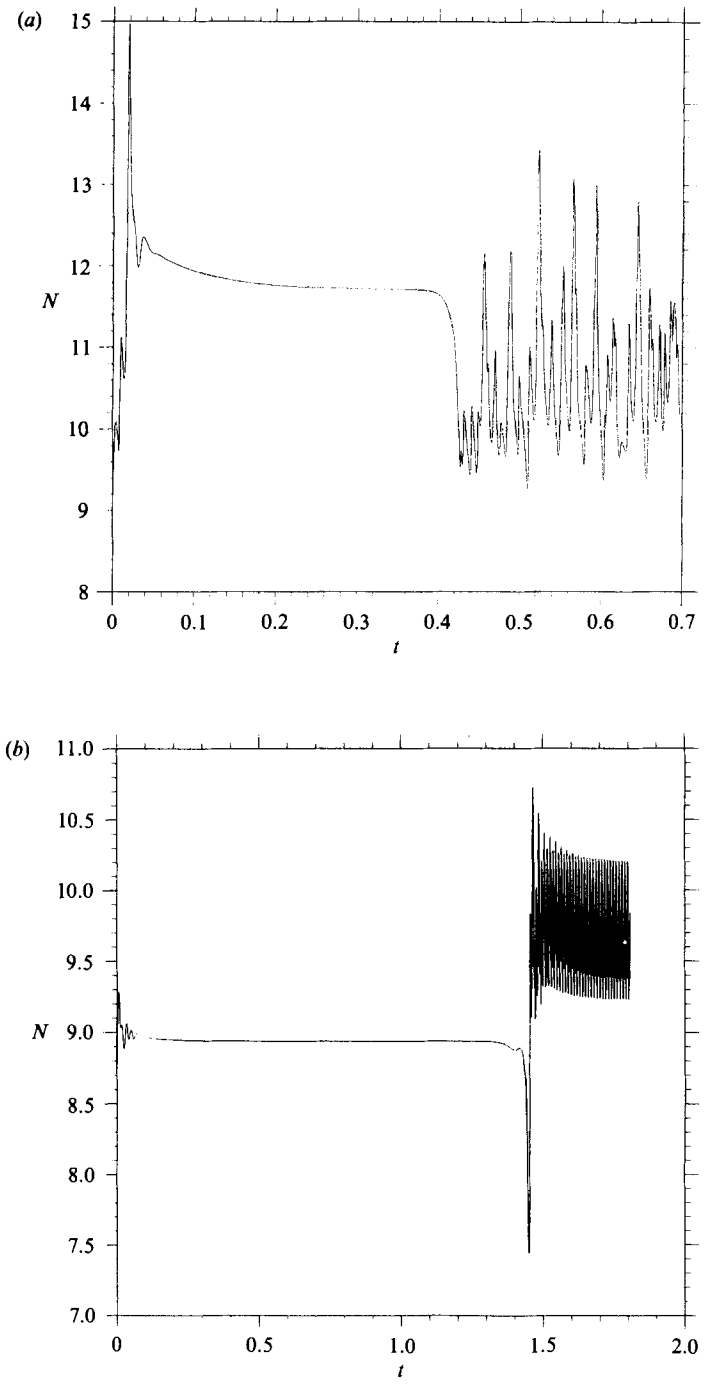

FIGURE 14. Abrupt transitions from one scale to another ($\lambda = 1.5$). (*a*) $N(t)$ for $R_1 = 9.1 \times 10^5$, showing the transition from the unstable steady 2^- solution to a chaotically varying solution with sinking plumes at both boundaries. (*b*) $N(t)$ for $R_1 = 5.1 \times 10^5$, showing the transition from the 2^+ branch to periodic oscillations about the 1^+ branch.

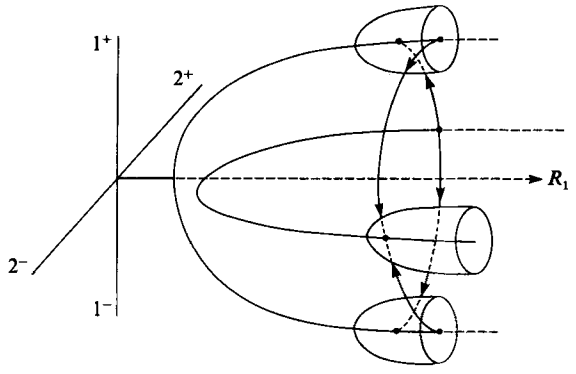

FIGURE 15. Sketch showing the relationship between solution branches in a three-dimensional space with two order parameters (corresponding to the amplitudes on the solution branches with $m = 1$ and 2) and a control parameter R_1.

behaviour was also obtained as the Rayleigh number was increased up to $R_1 = 1.8 \times 10^6$. In all these runs two sinking sheets remain anchored at $x = 0, 1.5$, and there are two rolls within the box. The thermal boundary layer is unstable and blobs grow and detach themselves in one roll or the other. As they do so the boundary between the two rolls migrates laterally to and fro, allowing more complicated motion than is possible for a single roll. Finally, there are the 2^+ solutions; figure 13(*c*, *d*) shows a stable steady solution at $R_1 = 3.1 \times 10^5$, with a single sinking sheet at $x = 0.75$ and two rolls symmetrical about that plane. As expected, the 2^+ branch becomes unstable at a lower Rayleigh number than the 2^- branch. When $R_1 = 5.1 \times 10^5$ perturbations that violate the symmetry about the midplane grow slowly and monotonically from the rounding error. $N(t)$ is shown in figure 14(*b*). At $t \approx 1.5$ there is an abrupt change; within one turnover time a sinking sheet forms at one of the lateral boundaries and there is a rapid transition to solutions with $l = 1.5$, which are periodic (as we saw in §5).

We are now able to assemble a picture of the bifurcations that occur for $\lambda = 1.5$. From table 3, $R_0^{(1)} < R_0^{(2)} < R_0^{(3)}$. The solutions with $m = 3$ appear last and become unstable first; somewhere around $R_1 = 10^5$ there is a transition to solutions on the 2^- branch. This process resembles the transition from three to two rolls in experiments on convection in liquid helium (Libchaber & Maurer 1982). The branches with $m = 1$ and 2 are shown schematically in figure 15. Here some measures of the amplitudes of solutions with one roll and two rolls in the box, such as the coefficients of terms proportional to $\sin(\pi x/\lambda)$ and $\sin(2\pi x/\lambda)$ in the Fourier series for ψ, are plotted against R_1. The 2^+ solutions become unstable around $R_1 = 4 \times 10^5$ and there is a transition to (periodic) solutions on either the 1^+ or 1^- branch. Steady solutions on the 2^- branch remain stable up to about $R_1 = 7 \times 10^5$. We conjecture that two successive Hopf bifurcations lead to quasi-periodic behaviour and a transition to aperiodicity by $R_1 = 9 \times 10^5$, and there is still a chaotic attractor in the neighbourhood of the 2^- branch at $R_1 = 1.8 \times 10^6$. Each of the two branches with $m = 1$ undergoes a Hopf bifurcation at $R_1 \approx 7 \times 10^4$. At $R_1 = 9 \times 10^5$ there are limit cycles near the branches. Cold blobs fall periodically from the boundary layer and the resulting plumes can waggle to and fro. We suspect that these two coupled oscillations are responsible for the quasi-periodic behaviour at $R_1 = 10^6$ (which is quite unlike that found with $\lambda = 1$) and that the route to chaos is by frequency locking and period doubling. Similar behaviour was found experimentally by Dubois

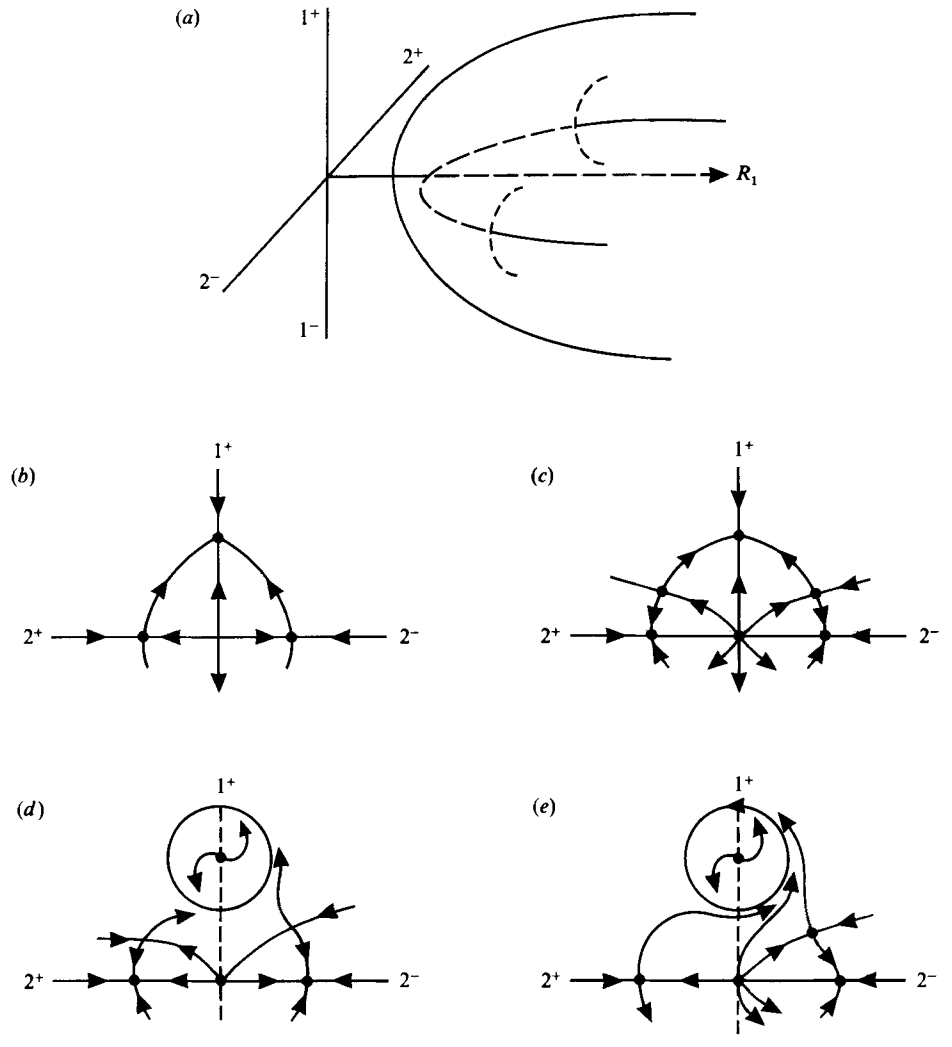

FIGURE 16. (*a*) Schematic bifurcation diagram in the three-dimensional space of figure 15 for $R_1 \leqslant 6 \times 10^4$, showing pitchfork bifurcations leading to the appearance of solution branches with $m = 1, 2$ and subsequent pitchfork bifurcations at which the branches with $m = 2$ gain stability. Corresponding phase portraits in the $1^{\pm}$–$2^{\pm}$ phase plane: (*b*) initial appearance of the non-stable solution branches with $m = 2$; (*c*) stabilization of the $m = 2$ branches, with the formation of non-stable mixed solutions. (*d*) Phase portrait showing behaviour at $R_1 = 9 \times 10^4$, after the first Hopf bifurcation. (*e*) Phase portrait showing behaviour at $R_1 = 5 \times 10^5$, with the stable 2^- solution, the non-stable 2^+ solution and a limit cycle enclosing the unstable solution with $m = 1$.

& Bergé (1980; Bergé *et al.* 1984). As R_1 increases, cold blobs develop nearer to the middle of the cell, as can be seen from our results for the 1^+ branch in figures 9–12. When subsidiary plumes form in the region $0 < x < \frac{1}{2}\lambda$ they are liable to be swept towards the left-hand boundary and to remain there. Hence there is a transition from $m = 1$ to the 2^- branch at $R_1 \approx 1.3 \times 10^6$.

This complicated picture can be summarized as follows. Steady solutions of types 1 and 2^- are unique in having no sinking plumes that are not at a boundary. For $\lambda = 1.5$ convection sets in with a pitchfork bifurcation leading to the two branches

with $m = 1$. As R_1 is increased, the next pitchfork bifurcation leads to the branches with $m = 2$ but solutions on both these branches are initially unstable. The corresponding bifurcation diagram is shown in figure 16(*a*) and the phase portrait in this regime is sketched in figure 16(*b*) (cf. Knobloch & Guckenheimer 1983). At some modest value of R_1 solutions with $m = 2$ gain stability through a (subcritical) pitchfork bifurcation, which leads to the appearance of saddle points, corresponding to the formation of four branches of non-stable mixed solutions. The corresponding phase portrait is sketched in figure 16(*c*). In this regime (which is not shown in figure 15 and has not been explored numerically) the four solutions with $m = 1, 2$ are all stable. A trajectory may be attracted to any one, depending on the initial conditions.

As R_1 is increased the 1^+ and 1^- solutions shed limit cycles. The nature of the oscillations, with two cold blobs circulating round each cell, implies that the oscillatory bifurcation involves mixed modes linking the solution branches with $m = 1$ to those with $m = 2$ (cf. §4 above). Hence the phase portrait at $R_1 = 9 \times 10^4$ can still be sketched in a plane containing the four solutions with $m = 1, 2$, as shown in figure 16(*d*). After an interval of chaos the 2^+ solution becomes unstable and the projected phase portrait at $R_1 = 5 \times 10^5$ is sketched in figure 16(*e*). Next, the 2^- solution loses stability and finally, for $R_1 \geqslant 1.4 \times 10^6$ all trajectories approach a chaotic attractor in the neighbourhood of the unstable 2^- solution.

We have confined our attention to boxes with $\lambda \leqslant 1.5$ when convection first sets in with $m = 1$. The complicated behaviour that we have described is associated with the transition from a state with a single sinking sheet at one of the lateral boundaries to a state with sinking sheets at both boundaries. By restricting the values of λ we were able to isolate and to recognize successive bifurcations. If $\lambda = 2$ convection first sets in with $m = 2$ and as λ is increased more rolls appear in the box. In a large-aspect-ratio box thermal boundary layers would still become unstable at high Rayleigh numbers, leading to an increase in the number of rolls present. Sinking plumes would be less constrained by lateral boundary conditions, so allowing a different and richer variety of dynamical behaviour which would be correspondingly more difficult to analyse. For similar reasons the behaviour found here will not necessarily recur in three-dimensional computations.

7. Discussion

Certain aspects of nonlinear convection are adequately represented by low-order systems of equations. For instance, the route to chaos by a cascade of period-doubling bifurcations (of which an example was given in §5) is familiar from third-order systems and can be explained by reference to one-dimensional maps. In this investigation we have tried to exploit dynamical systems theory in order to describe time-dependent behaviour in a convecting layer with non-trivial spatial structure. We find that instabilities in thermal boundary layers give rise to hot or cold blobs that circulate around a cell. After this Hopf bifurcation solutions must be simply periodic, so all cold blobs have to be equivalent. This constraint is broken at the next bifurcation, where the return map has an eigenvalue $\mu = \exp(2\pi i/q)$. For two blobs there is a strong resonance with $q = 2$ and the constraint can be broken by period-doubling or by a second Hopf bifurcation as we have seen. Subsequent bifurcations may then lead to chaos. With three blobs (as for example in the case described in §3) there is a wider range of possibilities. Period-doubling would imply that any specified blob recurred alternately in strong and weak forms, which could happen only if it was

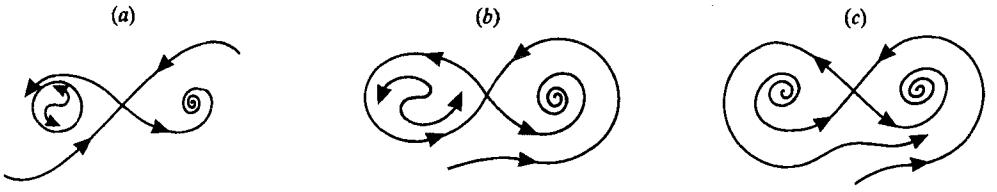

FIGURE 17. Simplified phase portraits showing the relationship between two fixed points, corresponding to rolls with different horizontal scales l, separated by a non-stable saddle point. (*a*) Appearance of a limit cycle about one unstable fixed point, which swells until (*b*) there is a homoclinic bifurcation, which might cause chaos, and (*c*) thereafter only one basin of attraction survives.

thermally brainwashed by diffusion. If its thermal memory persists we might expect the symmetry to be broken by a tripling of the period but the strong resonance with $q = 3$ involves a second Hopf bifurcation and quasi-periodicity. Four blobs might lose their symmetry by two successive period-doubling bifurcations or by one of the more exotic possibilities associated with the strong resonance with $q = 4$ (Arnol'd 1983). With five or more blobs the alternatives are period-doubling or quasi-periodicity followed by frequency-locking in the nonlinear regime. Thus the bifurcation pattern is affected by geometrical constraints. Similar effects arise with instabilities in differentially rotating systems, where the spatial symmetry can more easily be controlled (Hide 1958; Rabaud & Couder 1983), though nonlinear behaviour is restricted by the circular symmetry of the system (Rand 1982; Guckenheimer 1986).

The spatial structure illustrated here is predominantly associated with changes in cell size, and there is an obvious analogy with Taylor vortices (Di Prima & Swinney 1981; Benjamin & Mullin 1981, 1982; Cliffe & Mullin 1985). For low-amplitude convection such transitions can be described by simple evolution equations (Knobloch & Guckenheimer 1983). At higher Rayleigh numbers changes are produced by cold sheets falling from the upper boundary layer. We have seen that these sheets are constrained to behave with surprising regularity even when the disturbances are large.

We have explored transitions to temporal chaos without attempting to explain why chaos occurs. In many systems aperiodic oscillations are caused by homoclinic bifurcations (e.g. Sparrow 1982; Glendinning 1985; Knobloch *et al.* 1986) and we suspect that the same mechanism operates here too. Suppose that trajectories are projected onto a two-dimensional phase plane with two fixed points, corresponding to two states of the system (e.g. steady solutions on the 1^+ and 2^- branches in figure 16). If trajectories starting from infinity are attracted to one or other of these fixed points it follows that there must be a saddle point between them. Now suppose that one fixed point undergoes a Hopf bifurcation and sheds a limit cycle, as in figure 16(*d*). The resultant phase portrait is sketched in figure 17(*a*). As the stability parameter R_1 is increased the limit cycle swells until it becomes homoclinic to the saddle point, as shown in figure 17(*b*). Under certain conditions we expect to find chaotic behaviour in the neighbourhood of the homoclinic bifurcation at which the periodic orbit is destroyed. Then we would observe the following states as R_1 passed through successive bifurcation values: (i) two possible stable steady solutions, (ii) a stable periodic solution and a stable steady solution, (iii) chaotic oscillations about the first (unstable) solution and a stable steady solution, (iv) a single stable solution as in figure 17(*c*). Such behaviour is possible whenever there is a discontinuous

transition from one planform to another. In §5 we described the transition to chaos for $R_1 \approx 1.1 \times 10^5$. The interval of chaos was approached from either side by cascades of period-doubling bifurcations and this bubble structure is consistent with the simple picture outlined above. Low-order systems show an infinite sequence of such bubbles as the homoclinic orbit is approached. Here the sequence was apparently interrupted owing to the complicated spatial structure. More generally, therefore, we should imagine trajectories in a phase space with at least four dimensions, with separate basins of attraction for different types of solution (which may simultaneously be chaotic). As R_1 is increased more and more solution branches bifurcate from the trivial solution and the structure of phase space becomes difficult to visualize. Nevertheless, we conjecture that there exist many basins of attraction separated by non-stable fixed points, with possibilities of chaos associated with numerous homoclinic bifurcations.

In conclusion, we may speculate on the behaviour of other, less artificial, fluid systems in which spatial modes with smaller and smaller scales are excited as some stability parameter is increased. It has become fashionable to contrast two pictures of turbulence as though they were mutually exclusive. In one (due to Landau and Hopf) many different bifurcations are supposed to occur sequentially, generating extremely complicated quasi-periodic motion; in the other (due to Ruelle and Takens) everything is explained by a rapid transition to chaos after a few bifurcations (Hao 1984). Our results suggest that these two pictures need to be combined. Many independent spatial modes, with their associated bifurcations, are needed to describe the flow and there may be many different routes to chaos. Any chaotic attractor is bound to have a complicated structure which can only be described statistically, for example by discovering how its fractal dimension depends on the stability parameter.

We are grateful for comments from Paul Glendinning, Willem Malkus, Colin Sparrow, James Swift, Peter Swinnerton-Dyer and George Veronis. This research was supported by a grant from the Science and Engineering Research Council. Computations were carried out on the ULCC Cray-1 computer, with support from SERC and Imperial College. (Earth Sciences Contribution No. 1058.)

REFERENCES

ARNÉODO, A., COULLET, P. H. & SPIEGEL, E. A. 1985 The dynamics of triple convection. *Geophys. Astrophys. Fluid Dyn.* **31**, 1–48.

ARNOL'D, V. I. 1983 *Geometrical Methods in the Theory of Ordinary Differential Equations.* Springer. (Russian version, Moscow 1978.)

BENJAMIN, T. B. & MULLIN, T. 1981 Anomalous modes in the Taylor experiment. *Proc. R. Soc. Lond.* A **377**, 221–249.

BENJAMIN, T. B. & MULLIN, T. 1982 Notes on the multiplicity of flows in the Taylor experiment. *J. Fluid Mech.* **121**, 219–230.

BERGÉ, P. & DUBOIS, M. 1979 Study of unsteady convection through simultaneous velocity and interferometric measurements. *J. Phys. Lett.* **40**, L505–509.

BERGÉ, P., POMEAU, Y. & VIDAL, C. 1984 *L'Ordre dans le Chaos.* Hermann.

BOLTON, E. W., BUSSE, F. H. & CLEVER, R. M. 1986 Oscillatory instabilities of convection rolls at intermediate Prandtl number. *J. Fluid Mech.* **164**, 469–485.

BUSSE, F. H. 1967 On the stability of two-dimensional convection in a layer heated from below. *J. Math. Phys.* **46**, 140–150.

BUSSE, F. H. 1978 Nonlinear properties of thermal convection. *Rep. Prog. Phys.* **41**, 1929–1967.

BUSSE, F. H. 1981 Transition to turbulence in Rayleigh–Bénard convection. In *Hydrodynamics and the Transition to Turbulence* (ed. H. L. Swinney & J. P. Gollub), pp. 97–137. Springer.

CHANDRASEKHAR, S. 1961 *Hydrodynamic and Hydromagnetic Stability*. Oxford University Press.

CLEVER, R. M. & BUSSE, F. H. 1974 Transition to time-dependent convection. *J. Fluid Mech.* **65**, 625–645.

CLIFFE, K. A. & MULLIN, T. 1985 A numerical and experimental study of anomalous modes in the Taylor experiment. *J. Fluid Mech.* **153**, 243–258.

CURRY, J. H. 1978 A generalized Lorenz system. *Commun. Math. Phys.* **60**, 193–204.

CURRY, J. H., HERRING, J. R., LONCARIC, J. & ORSZAG, S. A. 1984 Order and disorder in two- and three-dimensional Bénard convection. *J. Fluid Mech.* **147**, 1–38.

DI PRIMA, R. C. & SWINNEY, H. L. 1981 Instabilities and transition in flow between concentric rotating cylinders. In *Hydrodynamic Instabilities and the Transition to Turbulence* (ed. H. L. Swinney & J. P. Gollub), pp. 139–180. Springer.

DUBOIS, M. & BERGÉ, P. 1980 Experimental evidence for the oscillators in a convective biperiodic regime. *Phys. Lett.* **76A**, 53–56.

FAUVE, S. 1985 Large scale instabilities of cellular flows. In *Chaos* (ed. G. Veronis & L. M. Hudon), pp. 55–69. Woods Hole Oceanogr. Inst. Tech. Rep. WHOI-85-36.

GLENDINNING, P. A. 1985 Homoclinic bifurcations. Ph.D. thesis, University of Cambridge.

GUCKENHEIMER, J. 1986 Strange attractors in fluids: another view. *Ann Rev. Fluid Mech.* **18**, 15–31.

GUCKENHEIMER, J. & HOLMES, P. 1983 *Nonlinear oscillations, dynamical systems and bifurcations of vector fields*. Springer.

HAO, B.-L. (ed.) 1984 *Chaos*, pp. 107–149. World Scientific.

HIDE, R. 1958 An experimental study of thermal convection in a rotating liquid. *Phil. Trans. R. Soc. Lond.* A **250**, 441–478.

HOCKNEY, R. W. 1970 The potential calculation and some applications. *Methods in Comp. Phys.* **9**, 135–211.

HOWARD, L. N. 1966 Convection at high Rayleigh number. In *Applied Mechanics* (ed. H. Görtler), pp. 1109–1115. Springer.

KELLER, J. B. 1966 Periodic oscillations in a model of thermal convection. *J. Fluid Mech.* **26**, 599–606.

KIMURA, S., SCHUBERT, G. & STRAUS, J. M. 1986 Route to chaos in porous-medium thermal convection. *J. Fluid Mech.* **166**, 305–324.

KNOBLOCH, E. & GUCKENHEIMER, J. 1983 Convective transitions induced by a varying aspect ratio. *Phys. Rev. A* **27**, 408–417.

KNOBLOCH, E., MOORE, D. R., TOOMRE, J. & WEISS, N. O. 1986 Transitions to chaos in two-dimensional double-diffusive convection. *J. Fluid Mech.* **166**, 409–448.

KNOBLOCH, E., WEISS, N. O. & DA COSTA, L. N. 1981 Oscillatory and steady convection in a magnetic field. *J. Fluid Mech.* **113**, 153–186.

KRISHNAMURTI, R. 1970 On the transition to turbulent convection. Part 2. The transition to time-dependent flow. *J. Fluid Mech.* **42**, 309–320.

LIBCHABER, A., FAUVE, S. & LAROCHE, C. 1983 Two parameter study of the routes to chaos. *Physica* **7D**, 73–84.

LIBCHABER, A. & MAURER, J. 1982 A Rayleigh–Bénard experiment: helium in a small box. In *Nonlinear Phenomena at Phase Transitions and Instabilities* (ed. T. Riste), pp. 259–286. Plenum.

LORENZ, E. N. 1963 Deterministic nonperiodic flow. *J. Atmos. Sci.* **20**, 130–141.

MCKENZIE, D. P., ROBERTS, J. M. & WEISS, N. O. 1974 Convection in the earth's mantle: towards a numerical simulation. *J. Fluid Mech.* **62**, 465–538.

MALKUS, W. V. R. 1972 Non-periodic convection at high and low Prandtl number. *Mem. Soc. R. Sci. Liège* (6) **4**, 125–128.

MASCHKE, E. K. & SARAMITO, B. 1982 On truncated-series approximations in the theory of Rayleigh–Bénard convection. *Phys. Lett.* **88A**, 154–156.

MOORE, D. R. 1988 Efficient explicit real FFTS for rapid elliptic solvers. *J. Comp. Phys.* (submitted).

MOORE, D. R., PECKOVER, R. S. & WEISS, N. O. 1974 Difference methods for time-dependent two-dimensional convection. *Comp. Phys. Commun.* **6**, 198–220.

MOORE, D. R. & WALLCRAFT, A. J. 1988 Rapid elliptic solvers for vector computers. *J. Comp. Phys.* (submitted).

MOORE, D. R. & WEISS, N. O. 1973*a* Two-dimensional Rayleigh–Bénard convection. *J. Fluid Mech.* **58**, 289–312.

MOORE, D. R. & WEISS, N. O. 1973*b* Nonlinear penetrative convection. *J. Fluid Mech.* **61**, 553–581.

NORMAND, C., POMEAU, Y. & VELARDE, M. G. 1977 Convective instability: a physicist's approach. *Rev. Mod. Phys.* **49**, 581–624.

PLOWS, W. H. 1968 Some numerical results for two-dimensional steady laminar Bénard convection. *Phys. Fluids* **11**, 1593–1599.

POMEAU, Y. & MANNEVILLE, P. 1980 Intermittent transition to turbulence in dissipative dynamical systems. *Commun. Math. Phys.* **74**, 189–197.

RABAUD, M. & COUDER, Y. 1983 A shear-flow instability in a circular geometry. *J. Fluid Mech.* **136**, 291–319.

RAND D. 1982 Dynamics and symmetry: predictions for modulated waves in rotating fluids. *Arch. Rat. Mech. Anal.* **79**, 1–37.

ROBERTS, G. O. 1979 Fast viscous Bénard convection. *Geophys. Astrophys. Fluid Dyn.* **12**, 235–272.

ROBERTS, P. H. 1967 Convection in horizontal layers with internal heat generation. Theory. *J. Fluid Mech.* **30**, 33–49.

SCHNECK, P. & VERONIS, G. 1967 Comparison of some recent experimental and numerical results in Bénard convection. *Phys. Fluids* **10**, 927–930.

SPARROW, C. T. 1982 *The Lorenz Equations: Bifurcations, Chaos and Strange Attractors.* Springer.

SPARROW, E. M., GOLDSTEIN, R. J. & JONSSON, V. K. 1964 Thermal instability in a horizontal fluid layer: effect of boundary conditions and nonlinear temperature profile. *J. Fluid Mech.* **18**, 513–528.

SPIEGEL, E. A. 1971 Convection in stars. I, Basic Boussinesq convection. *Ann. Rev. Astron. Astrophys.* **9**, 323–352.

THIRLBY, R. 1970 Convection in an internally heated layer. *J. Fluid Mech.* **44**, 673–693.

TREVE, V. M. & MANLEY, O. P. 1982 Energy conserving Galerkin approximations for 2-D hydrodynamic and MHD Bénard convection. *Physica* **4D**, 319–342.

VERONIS, G. 1966 Large amplitude Bénard convection. *J. Fluid Mech.* **26**, 49–68.

WALDEN, R. W., KOLODNER, P., PASSNER, A. & SURKO, C. M. 1984 Nonchaotic Rayleigh–Bénard convection with four and five incommensurate frequencies. *Phys. Rev. Lett.* **53**, 242–245.

WEISS, N. O. 1981 Convection in an imposed magnetic field II. The dynamical regime. *J. Fluid Mech.* **108**, 273–289.

WELANDER, P. 1967 On the oscillatory instability of a differentially heated fluid loop. *J. Fluid Mech.* **29**, 17–30.